FACULTY OF INFORMATION TECHNOLOGY AND ELECTRICAL ENGINEERING
DEGREE PROGRAMME IN ELECTRONICS AND COMMUNICATIONS ENGINEERING

MASTER'S THESIS

RELIABILITY PERFORMANCE ANALYSIS OF HALF-DUPLEX AND FULL-DUPLEX SCHEMES WITH SELF-ENERGY RECYCLING

Author	Dian Echevarría Pérez
Supervisor	Assist. Prof. Hirley Alves
Second Examiner	Assist. Prof. Onel L. Alcaraz López

March 2021

Echevarría Pérez D. (2021) Reliability performance analysis of half-duplex and full-duplex schemes with self-energy recycling. University of Oulu, Degree Programme in Electrical Engineering, 67 p.

ABSTRACT

Radio frequency energy harvesting (EH) has emerged as a promising option for improving the energy efficiency of current and future networks. Self-energy recycling (sER), as a variant of EH, has also appeared as a suitable alternative that allows to reuse part of the transmitted energy via an energy loop. In this work we study the benefits of using sER in terms of reliability improvements and compare the performance of full-duplex (FD) and half-duplex (HD) schemes when using multi-antenna techniques at the base station side. We also assume a model for the hardware energy consumption, making the analysis more realistic since most works only consider the energy spent on transmission. In addition to spectral efficiency enhancements, results show that FD performs better than HD in terms of reliability. We maximize the outage probability of the worst link in the network using a dynamic FD scheme where a small base station (SBS) determines the optimal number of antennas for transmission and reception. This scheme proves to be more efficient than classical HD and FD modes. Results show that the use of sER at the SBS introduces changes on the distribution of antennas for maximum fairness when compared to the setup without sER. Moreover, we determine the minimum number of active radio frequency chains required at the SBS in order to achieve a given reliability target.

Keywords: Full-duplex, Maximal ratio combining, Maximal ratio transmission, Self-energy recycling, Ultra-reliable communications.

TABLE OF CONTENTS

FOREWORD

This thesis mainly focuses on the reliability performance of half-duplex (HD) and full-duplex (FD) schemes when using self-energy recycling (sER). This work was completed at the Centre for Wireless Communications (CWC). First of all, I would like to express my gratitude to my supervisor Assist. Prof. Hirley Alves for the opportunity of being part of the MTC group and for his unconditional support in my studies and work. A special thanks to Assist. Prof. Onel L. Alcaraz López, who has always guided me through every step since I joined CWC and has been available when I have needed his help.

I am also grateful to my friends and colleagues Osmel and Nelson since we have faced difficult situations together and supported each other through those moments. Also thanks to all my colleagues in the MTC group for maintaining a supportive work environment.

Back in Cuba, I would like to thank my family for always supporting me throughout my life, especially my parents and grandparents. I also thank my brothers who have motivated me to go ahead no matter what.

A special thank goes to my wife and children, who have been far from me all this time but have provided me the strength to go on, that is why I dedicate this work to them.

This research has been financially supported by Academy of Finland, 6Genesis Flagship (Grant no. 318927), EE-IoT (no. 319008).

Oulu, 11th March, 2021

Dian Echevarría Pérez

LIST OF ABBREVIATIONS AND SYMBOLS

2G-6G	Second to sixth generation of mobile communications
ADC	Analog-to-digital conversion
AF	Amplify-and-forward protocol
AP	Access point
BS	Base station
CDF	Cumulative density function
CSI	Channel state information
CSMA/CA	Carrier sense multiple access with collision avoidance
Cx	Communication
DAC	Digital-to-analog conversion
DC	Direct current
DL	Downlink
DSP	Digital signal processing
DSSSC	Distributed secure switch-and-stay combining
EE	Energy efficiency
EGC	Equal gain combining
EH	Energy harvesting
EM	Electromagnetic
eMMB	Enhanced mobile broadband
ET	Energy transmitter
ER	Energy receiver
FD	Full-duplex
GL	Gauss-Laguerre
GPD	Generalized Pareto distribution
HAP	Hybrid access point
HARQ	Hybrid automatic repeat request
HD	Half-duplex
IoT	Internet of Things
LOS	Line-of-sight
MAC	Medium access control
MIMO	Multiple-input multiple-output
MISO	Multiple-input single-output
ML	Machine learning
mMIMO	Massive MIMO
MMSE	Minimum mean square error
mMTC	Massive machine-type communication
MRC	Maximal ratio combining
MRT	Maximal ratio transmission
NB-IoT	Narrowband IoT
NOMA	Non-orthogonal multiple access
OFDM	Orthogonal frequency-division multiplexing
OFDMA	Orthogonal frequency-division multiple access
PA	Power amplifier
PDF	Probability density function
PB	Power beacon

PS	Power splitting
RF	Radio frequency
RFID	RF identification
RV	Random variable
Rx	Reception
SBS	Small BS
SC	Selection combining
SDMA	Time-division multiplex access
SE	Spectral efficiency
sER	Self-energy recycling
SI	Self-interference
SIC	SI cancellation
SINR	Signal-to-interference-plus-noise radio
SNR	Signal-to-noise radio
SSC	Switch-and-stay combining
SWIPT	Simultaneous wireless information and power transfer
TDMA	Time-division multiplex access
TS	Time switching
Tx	Transmission
UL	Uplink
URC	Ultra-reliable communications
URLLC	Ultra-reliable low-latency communications
WEH	Wireless EH
WPC	Wireless powered communications
WPCN	Wireless powered communications networks
WPT	Wireless power transfer
WSN	Wireless sensor networks

$\Gamma(\cdot)$	Upper incomplete gamma function and Gamma distribution
$\beta(\cdot)$	Beta function
λ	Wavelength or parameter of the exponential distribution
ξ	Outage probability target
$\|\|\cdot\|\|$	Norm operator
$(\cdot)^T$	Transpose operator
$(\cdot)^H$	Complex conjugate operator
$E\{\cdot\}$	Expected value
$\mathbb{P}\{\cdot\}$	Outage probability
${}_1F_1(\cdot)$	Confluent hypergeometric function of first kind
${}_2F_1(\cdot)$	Gauss hypergeometric function

1 INTRODUCTION

The beginning of every generation of wireless communication systems comes with new high-level requirements. Fifth and beyond generations of mobile communications are not the exception. New operation modes have been defined for them: massive machine-type communications (mMTC), ultra-reliable low-latency communications (URLLC, or critical MTC [1]) and enhanced mobile broadband (eMBB) [2]. Each of these modes encloses a group of implicit characteristics (Figure 1) that allows the development of cutting-edge applications. Industry automation, smart cities and augmented reality (see Figure 2 for more examples) are some of the well known uses cases present in the literature, just to name a few [3–6]. For them, high reliability, energy efficiency (EE) and spectral efficiency (SE) become critical aspects, respectively.

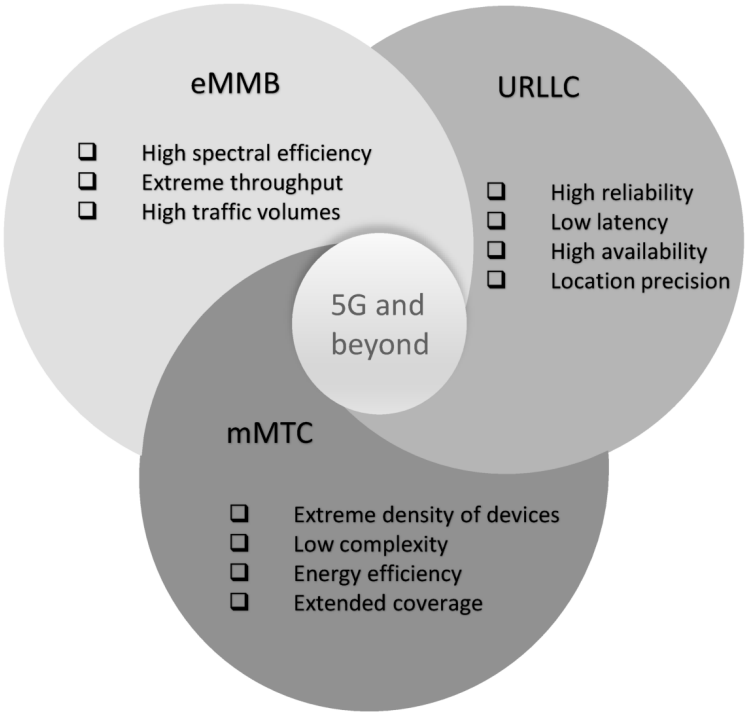

Figure 1. Operation modes of 5G and beyond wireless networks.

1.1 Ultra-reliability in 5G and future networks

As illustrated in the figures, services such as smart traffic, self-driving cars, remote surgery, etc, enclose strict requirements in terms of reliability, i.e., packet error rates that are below 10^{-5}, and up to 10^{-9}, almost 100 % of the time. However, the specific lower limit on the error probability depends on the service in question [7,8]. Some applications and the corresponding error requirements are: vehicle-to-vehicle communications and teleprotection in smart grids - 10^{-5} [7, 9], industry automation - 10^{-9} [10] and remote surgery - 10^{-9} [9]. Together with the error rate, the outage probability is also an effective metric for measuring ultra-reliability [8]. On the other hand, reliability is affected by a

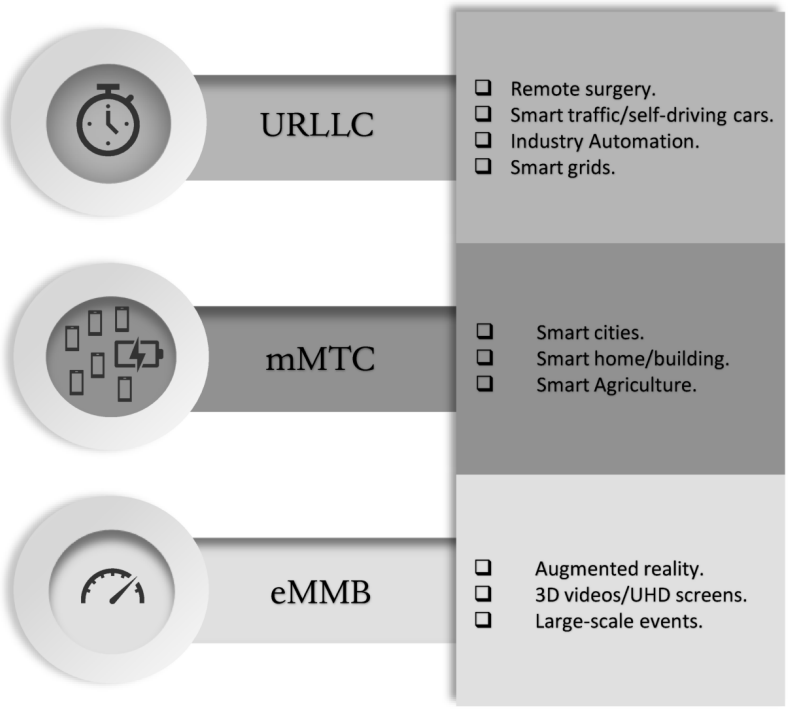

Figure 2. Uses cases of 5G and future wireless networks.

diverse group of factors, for instance, collisions due to simultaneous access to the channel of several users. Moreover, interference from users in adjacent channels, coexistence in the same frequency band and synchronization issues also affect the reliability [11]. These elements cannot be faced only using techniques implemented in previous generations of mobile communications, say, 2G, 3G and 4G, thus, the ambitious goals in error probabilities would not be achieved. Instead, the existing state-of-the-art advancements must be combined with new enablers to go below the minimum 10^{-5} target for ultra-reliable communications (URC). It is worth pointing out that URC focuses on the reliability part of URLLC, ignoring the requirements in terms of latency.

1.1.1 Enablers for URC

Spatial diversity is a key enabler for achieving URC, although it is strongly conditioned on the acquisition of the channel state information (CSI); which is an aspect further commented below. Multiple-input multiple-output (MIMO) offers opportunities to URLLC since the large number of antennas translates to high signal-to-noise radio (SNR) links, quasi-deterministic and quasi-immune to fading. It also brings high spatial multiplexing capabilities [8], thus, taking error probabilities to low levels. The issue of CSI acquisition has been widely studied for the past years and it represents a critical point for URC since a bad channel estimation leads to higher error probabilities. Several models dealing with partial/imperfect CSI or based on statistics of the channel have been proposed in the literature [12–14]. Nevertheless, solutions based on machine learning

(ML) seem to be one of the most promising alternatives in the near future. ML is considered as a potential enabler that has opened a new world of opportunities, including the so-called predicted URLLC. The inclusion of ML improves the communication reliability provided properly designed solutions [15]. Base station (BS) densification also appears as an important aspect that contributes to achieve ultra-reliability, this comes from the fact that a higher number of BSs allows the users to associate with their neighboring BSs in a more efficient way, providing better resource allocation at shorter distances [8]. Reliability can also be improved by using low-rate codes and retransmissions for error correction [11]. Other enablers such as network slicing, intelligence at the edge, transmission time interval and hybrid automatic repeat request (HARQ) roundtrip time, and grant-free random access have been studied recently, although they mainly focus on latency aspects [16].

1.2 EE for 5G and beyond

Figure 1 also highlights EE as a characteristic of future networks, with special relevance to enable sustainable Internet of Things (IoT). In the coming years, billions of devices will be connected to the Internet, for instance, sensors, actuators, radio-frequency identifiers (RFIDs), mobile phones, etc, which would be periodically receiving/sending information. Note that maintenance tasks to a huge amount of terminals would be difficult or impractical. One of the most common maintenance tasks is battery replacement after depletion, since most of these devices have batteries as their main power unit. However, battery replacement would be tricky and hazardous in several scenarios, for example, sensors in an industrial environment, sensor implanted in the human body (body area networks) or others embedded in building structures. Then, the continuous substitution of the energy sources becomes a high cost task, which requires a lot of time and represents an environmental problem [17]. Hence, it is required to come up with new technologies that contribute to avoid these issues. Several efforts have been conducted in terms of EE for the last few years, even new low-power-consuming solutions have been proposed in terms of connectivity. Here, technologies such as Lora/LoraWAN, SigFox [18], narrowband IoT (NB-IoT) [19] and Zigbee [20] have played a key role as pioneers in the IoT market. EE, however, cannot be seen as a requirement only at the side of the end device. Instead, it is a concept that must be applied throughout the network, including the BSs.

Under the paradigm of 'green communications', energy harvesting (EH) solutions and hardware improvements in conjunction with energy-efficient communication techniques seem to be the key to achieve EE.

1.2.1 Hardware improvements and energy-efficient communication techniques

One of the first metrics used for evaluating the EE was the ratio between the throughput and the total energy consumption, in bits/Joule, including the energy spent for radio frequency (RF), the energy consumed by the power amplifiers and energy dissipated in other circuit blocks. The main drawback of the previous criterion is that it applies

only for a single link. Hence, other more encompassing metrics may be considered, for instance, network benefit-cost ratio, which is simply the ratio between the sum of all throughputs of each link in the network and the total power consumption. The main problem of this approach is that it does not allow to adjust the EE of individual devices. In order to overcome this issue, a broader criterion is proposed [21]. It is based on a multi-objective optimization to maximize the combination of all individual EEs through some predefined functions (weighted sum EE, weighted product EE [22], etc).

The hardware has been always the most critical point in terms of energy consumption, which is why it is required to design circuits with low power utilization while keeping the required standards. Design of more efficient RF chains, simplified transceivers and the implementation of network virtualization push forward high-level improvements in EE [21]. Power amplifiers have also been optimized, and state-of-the-art designs that aim at achieving lower peak-to-average-power ratio have been proposed in [23, 24]. The insertion of intelligent reflecting surfaces in the search of more efficient wireless solutions has opened new possibilities for hardware improvements. Their reflecting properties, which can be controlled, have been object of continuous research, e.g., [25–27].

On the other hand, resource allocation seems another viable option for improving the EE in current and future wireless networks [28–31]. Likewise, within the framework of energy-efficient communication techniques, radio optimization, clock synchronization and efficient wake-up/sleep schemes enclose a series of strategies for EE. Moreover, routing schemes and data reduction strategies complement the previous group of possible solutions [32]. Table 1 shows a set of approaches for EE and the group they belong to.

Table 1. Energy-efficient communication techniques.

Scheme	EE technique
Radio optimization	Transmission power control [33] Modulation optimization [34] Energy-efficient Cognitive Radio [35] Cooperative Communication [36] Beamforming [37, 38]
Clock synchronization	Transmission scheduling [39] Data fusion [40] Power management [32]
Efficient Wake-up/Sleep modes	Duty cycles [41, 42] Topology control [43] Passive wake-up radios [44]
EE routing	Multipath routing [45, 46] Clustering [47, 48] Relay deployment [49]
Data reduction	Aggregation [50] Network coding [46, 51] Data compression [52]

1.2.2 EH solutions

With the advancements in the field of green communications, EH has become a potential enabler for more energy-efficient wireless systems. It allows the devices to replenish their batteries in order to extend their lifetime using clean energies. There are plenty of EH techniques, which can be grouped into five major classes: mechanical EH, thermal EH, EH from fluid flow, radiant EH and wireless EH (WEH). Detailed description of these categories is added below.

- Mechanical EH: The use of the so-called piezoelectric materials allow the conversion of any mechanical movement into electricity, for instance vibrations, pressure variations, etc [32].

- Thermal EH: This is a mode of EH where thermoelectric materials are used to convert heat into electricity. It is quite simple to implement and offers high reliability. The main issue is that conversion efficiencies are relative low, up to 10% [53].

- EH from fluid flow: The production of energy from the fluids has shown a huge potential. It came true thanks to the discovery of the energy transduction from the movement of ionic liquids and the use piezoelectric materials. Devices designed under these principles are know as piezoelectric energy harvesters [54].

- Radiant EH: Within this category, the harvesting process from the light and RF wireless power transfer (WPT) are included (the latter is covered in WEH since it fits in both categories). Clearly, solar light constitutes one of the most common alternative energy sources nowadays. The development of technologies using semiconductor materials has allowed the design of more efficient solar panels with power densities up to 100 mW/cm^2. It is commonly used for outdoors but technologies for indoors using artificial light have been developed as well, although with lower levels of efficiency [55].

- WEH/wireless power transfer (WPT): This category becomes suitable for powering devices where none of the previous technologies is available. WEH refers to the techniques applied in order to capture the energy, while WPT is the group of approaches where dedicated sources are used to transfer energy to end devices, i.e., WPT and WEH are applied at opposite sites of the network. WPT is divided into three subcategories: inductive coupling, magnetic resonance coupling and electromagnetic (EM)/microwave radiation [32]. Inductive and magnetic resonance coupling work in the near field region whereas EM/microwave radiation is more suitable for the far field region.

  - Inductive coupling: This a wireless charging technology that covers small distances, usually in the range of a few centimeters from the transmitter and is based on the magnetic field induction principle, which allows to transfer energy between two coils. In short, a varying voltage/current at the source coil generates a varying magnetic field that induces a voltage/current at the secondary coil. This current is used to charge devices provided that the distance between the coils is short, otherwise the efficiency drops sharply.

Usually the secondary coil is tuned to the operating frequency in order to improve the efficiency. The main advantages of this technology are its simplicity for implementation and efficiency at short distances [56, 57].

- Magnetic resonant coupling: A magnetic resonant coupling system uses a pair of coupled coils with an extra capacitance, which makes the transmitter and the receiver resonate at the same frequency. It operates at larger distances than inductive coupling at the cost of flexibility and complexity because it is optimized for certain distances and circuit alignment settings. Efficiencies above 90 % have been proved for distances smaller than 30 cm [58]. One of the main advantages of this technology is that allows to charge multiple receivers using a single transmitter [57].
- EM/microwave radiation: This is a mode of EH where the energy is conveyed by the RF signals. These signals propagate at the speed of light either isotropically or as beams. Isotropic radiation is more useful for broadcast scenarios and beams for point to point connections using antenna arrays at the transmitter side. The efficiency of these systems depends on the distance (proportional to the inverse of squared distance), the presence of line-of-sight (LOS) and the energy density at the receive antenna. The usual range of frequencies for applications using EM/microwave radiation is from 300 MHz to 300 GHz. Other electromagnetic waves can be used, for example x-rays, but for safety measures they are not widely used [57]. Receivers are simple, with small dimensions (ex. RFIDs), equipped with an antenna plus rectifying circuit (rectenna) and some additional processing blocks [59, 60].

1.3 Thesis contribution

Most of existing works in full-duplex (FD) wireless-powered communications focus on optimizing network parameters such as rates, EE, reliability, among others. Many of them do it through properly setting beamforming vectors, power allocation, etc. For the particular case of EE, the use of self-energy recycling (sER) at the BS side has not been a common practice, which however needs to be considered for improving the EE. Moreover, the benefits of sER for URC have not been considered either at that side of the network. It is also common to improve the reliability by adding more antennas or increasing transmit power when possible in both FD and half-duplex (HD) scenarios. What has not been considered to the best of the author's knowledge, is the use of dynamic antenna allocation between transmission and reception at the FD BS. Furthermore, the energy consumption of the active elements is usually not considered for simplicity, but it is a design parameter required for any practical implementation. Different from state-of-the-art works, herein we compare the performance of HD and FD architectures with the presence of sER at the SBS while the power consumed on the RF chains is considered. We analyze the outage probability and aim at guaranteeing the maximum reliability fairness between uplink (UL) and downlink (DL) channels. The fairness is achieved by minimizing the maximum outage probability. For this purpose, we propose a dynamic FD approach which determines the optimum number of transmit and receive antennas under different network configurations. This flexibility level is possible due to the use of state-of-the-art transceivers, where antennas can switch indistinctly between transmission and reception.

We prove that the dynamic FD schemes outperform HD and rigid FD, thus evidencing its outstanding performance in terms of outage probability in all network configurations under evaluation. We also analyze the benefits of using sER, as well as its influence on the optimal configuration of the proposed FD scheme.

1.4 Thesis outline

The remaining of the thesis is structured as follows:

- **Chapter 2**: Discusses the principles of FD communications and compares FD and HD. It also introduces the concepts behind RF WEH and sER and also covers the fundamentals of diversity as enabler for URC.
- **Chapter 3**: Introduces the system model and derives the mathematical expression for the outage probability in both HD and FD schemes.
- **Chapter 4**: Discusses the results and validates the improvements of the proposed scheme in terms of outage probability.
- **Chapter 5**: Concludes the thesis and comments on future extensions.

2 SELECTED ENABLERS FOR SPECTRAL AND ENERGY EFFICIENT RELIABLE COMMUNICATIONS

2.1 Full-duplex communications

FD has emerged as a promising technology for future wireless networks since it brings improvements in terms of SE. Concisely, the SE is doubled with compared to classical HD systems since both transmission and reception occur simultaneously in the same frequency. The main issues in FD are related to the power leakage that arises between transmit and receive antennas, this phenomenon is called self-interference (SI). Figure 3 illustrates the functioning of both HD and FD modes. If the communication is divided in time intervals, we can notice how FD devices operate. In a nutshell, a FD device transmits and receives information all the time with the presence of SI links. On the

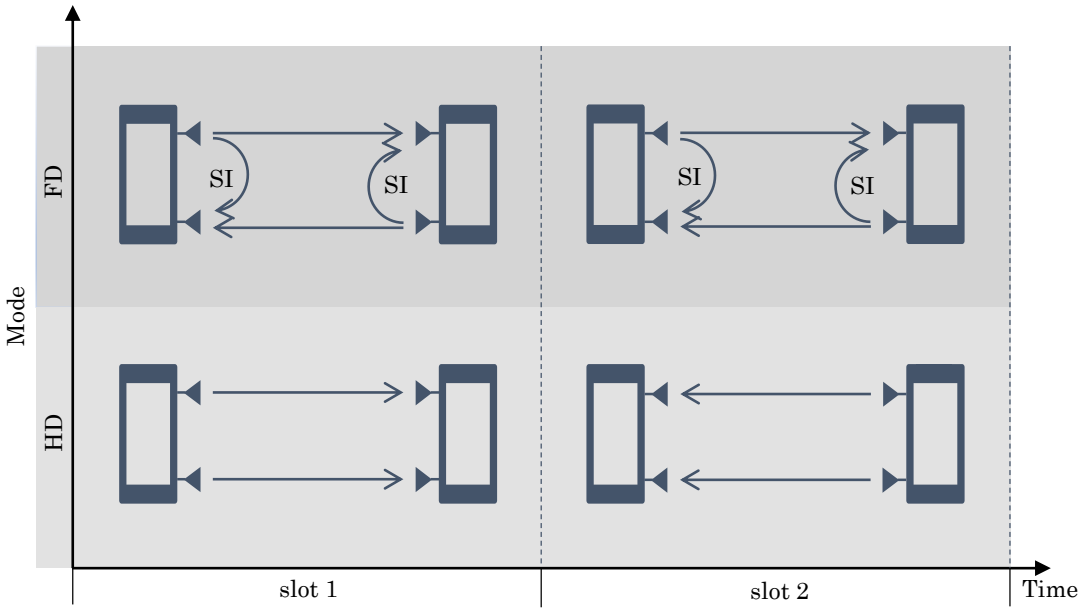

Figure 3. Graphic description of HD and FD modes.

other hand, in HD, one of the time intervals is used for transmission and the next one for reception. Since all antennas transmit or receive at once, HD does not have to deal with SI. Schemes that intend to reduce the SI levels are termed as SI cancellation (SIC) techniques.

In the case of practical FD radios, designs can either use shared or separated antennas for both transmission and reception. In a separated architecture, transmit RF chains use dedicated radiating antennas whereas receive RF chains use dedicated sensing antennas. In a shared architecture, transmit and receive RF chains share the same set of antennas. Sharing the same antennas requires the use of the so-called 'circulator', which is a three-port ferrite device that transports the RF signals from one port to another [61]. Several works have focused on FD communications, dealing with SIC, FD radios, FD relays in cooperative networks, FD protocols, etc [62–87].

2.1.1 SIC techniques

As mentioned before, SI is nothing but the incidence of the transmit signal on the receive antenna (60 - 100 dB higher than the desired signal [83]), which interferes with the receive signal, thus causing a huge degradation of the signal-to-interference-plus-noise radio (SINR). In order to overcome this issue, several SIC techniques have been proposed. They are grouped into two different categories named as: active and passive cancellation [67].

- Passive SIC: These techniques are based mainly on antenna separation, antenna placement or cross-polarization. They mainly take advantage of physical properties of the electromagnetic waves and propagation medium.

  Antenna separation: In this case, as the name suggests, SIC is based on the distance between transmit and receive antennas. This is the most common approach for SIC since takes advantage of the path loss due to the distance and surrounding objects. It is also quite common to use shielding plates in order to block direct paths introducing additional losses to signals. The main benefits of this techniques rely on the simplicity and the spatial separation between links. However, the introduction of shielding plates can also affect the desired signal. Furthermore, it might not be appropriate for devices with a small form-factor. Attenuation in the order of 30 dB is attainable using this approach [67]. According to [84], 40 dB of attenuation is possible for separation of 6 - 8 inches, although, higher levels are achievable if antennas are placed further away, as discussed in [85].

  Antenna placement: In this case a minimum of three antennas is required, two for transmission and one for reception. The operation principle is straightforward, the receive antenna is placed at a distance d from one transmit antenna and at $d + \lambda$ (λ represents the wavelength) from the other. This strategy will cause a null effect around the position of the receive antenna since the signals will add up destructively. However, there are a few issues to be considered before implementation, this approach is not beneficial for devices with small form-factor and requires manual tuning. For instance, for a device operating at 2.4 GHz, $\lambda = 12.5$ cm, which is higher than the size of many wireless devices. Attenuation levels up to 30 dB are achievable according to [66], although [67] states that 47 dB are also attainable. Higher SICs values are possible in conjunction with the use of active techniques. The use of antenna placement in MIMO systems has also been considered in the literature [63, 86].

  Cross-polarization: It is based on the electromagnetic principles behind antenna theory. For maximum energy transfer between two antennas, the polarization between them must be the same (horizontal, vertical, etc). The polarization determines the direction of the electric field radiated by the antenna. The more aligned the fields, the larger the effective energy transfer. The opposite happens when there is mismatch between polarizations. For example, using vertical polarization (is a variant of linear polarization together with horizontal) at the transmitter side and horizontal at receiver side would cause a theoretical total

isolation. This technique has the drawback that the environment can affect the polarization, hence, producing mismatches at either side. The main advantage is that small form-factor devices turn an appropriate target for cross-polarization approaches [67]. A couple of practical implementations are proposed in [87, 88].

Other techniques are available in the literature, for example, directional passive suppression, which guarantees up to 30 dB of attenuation. Such level is reached avoiding the intersection of the radiation patterns of transmit and receive antennas [66]. Passive SIC, in general, does not provide the required SIC levels for feasible communications, which becomes even more difficult with the current trend in the electronic industry of designing small form-factor devices. This fact is incompatible with passive schemes, which require considerable antenna separation in most cases.

- Active SIC: Active schemes base their functioning mainly on processing carried out by analog circuits of the RF chains and the digital circuits after analog-to-digital (ADC) conversion. They are classified in analog SIC and digital SIC domains. Combinations of them are possible, and in general improve the performance. This option is termed as hybrid SIC.
  Analog domain: It consists in subtracting a predicted received signal from the received one before the ADC, when the signal is still on the RF chain. We could think that to obtain the desired signal at reception, we should just subtract the transmitted from the received one, but in practice is not that easy. This is because the circuitry of the transmit RF chain and all the processing introduce levels of distortion and noise. Moreover, the transmitted signal impinges upon surrounding objects and is reflected, hence at the receive antenna we will have a strong LOS component (SI link) plus some additional copies of the signal. In this regard, [64] proposes a dynamic algorithm to estimate the distortion introduced by the ciruits and accurately model the SI. Analog schemes are also classified into adaptive or non-adaptive, depending on the possibilities they have to tune their parameters due to changes in the environment. Adaptive approaches can adjust parameters such as gain, delay and phase automatically in the SI prediction process while non-adaptive schemes must rely on manual tuning of such parameters. New analog SIC mechanisms have been proposed, for instance, in [75] authors uses the signal at the circulator that has been reflected by the antenna, in order to cancel the SI, achieving up to 40 dB of SIC. On the other hand, a new approach is presented in [69], where an extra RF chain is required to generate the cancellation signal, such signal is used at the receive RF chain for SIC, reaching up to 48 dB of attenuation. Analog SIC suppresses both noise and signal, it is easy to implement and compensates for multipath propagation. The estimation of the SI is one of the main drawbacks for analog SIC.
  Digital domain: Digital techniques are usually employed after analog SIC. Once analog SIC is applied, a residual SI signal remains since these mechanisms attenuate the SI partially (they are unable to take the SI to the noise floor by themselves), hence this residual SI has to be further cancelled. Digital SIC is performed after ADC using digital signal processing (DSP) techniques. Levels of cancellation up to 10 dB can be achieved when using digital approaches alone, and up to 60 dB when combined with analog SIC [67]. However, recent studies have proved that

higher levels are attainable. For instance, the proposal presented in [64] guarantees up to 110 dB of SIC for a WIFI radio in noisy environments, closely doubling the system throughput. In [77], it was stated that values above 100 dB are possible in realistic environments for FD relays with bandwidths as high as 80 MHz. The main advantage of digital SIC is that it contributes to mitigate the residual SI after analog cancellation. The increment in the quantization noise as well as the limited cancellation capabilities are highlighted as the principal downsides.

Other well discussed issue is the modeling of the SI channel and the residual SI. The SI channel is usually modeled as Rician distributed with a high LOS factor, which means that the channel behaves in a quasi-deterministic way [62,78,89]. On the other hand, the residual SI has been modelled as Rician distributed with a small LOS factor [62,79] and with Nakagami-m fading [80]. Other distributions have also been derived, as in [81].

2.1.2 Comparison of HD and FD

It is worth highlighting both the advantages and disadvantages of FD when compared to classical HD technology. FD offers a series of advantages, some of them are listed below

- **Higher throughput**: FD can in theory double the throughput of HD shemes.
- **Improved end-to-end delay**: FD reduces the end-to-end delay in relay networks. The use of relay nodes operating in FD reduces the delay of the transmitted signal since relays transmit and receive information simultaneously, hence, they do not have to wait to the next time interval for transmission as in HD.
- **Better network secrecy**: FD enhances network secrecy at physical layer. The simultaneous presence of two signals at the same frequency makes difficult for an eavesdropper to decode the information [82].
- **Collision avoidance**: It also provides collision avoidance since carrier sense multiple access with collision avoidance (CSMA/CA) in classical HD schemes requires the devices to sense the medium previous transmission, whereas in FD only the first device that starts transmitting needs to sense the channel quality [66].

However, not everything is positive when selecting FD as the operation mode, its implementation comes at the cost of some negative aspects. These are:

- **Higher hardware complexity**: The complexity of the FD hardware is higher if compared to HD. The hardware requirements for analog SIC and the required computational capabilities for digital SIC make the design of FD radios a difficult task.
- **Higher power consumption**: The increment in the hardware complexity and the required processing for SIC increases the power consumption.
- **Imperfect SIC**: The estimation of the SI channel is a critical point for SIC, hence, failures in the implementation of reliable SIC techniques lead to a low performance in FD.

- **Higher packet loss rate**: FD schemes have to process a larger number of packets than HD due to concurrent transmission and reception. This fact leads to higher number of loss packets [66].

2.2 RF wireless-powered communications

RF WPT is an attractive solution for powering massive sensor networks. As mentioned in the previous chapter, harvesting energy from renewable energy sources in the environment is an alternative for reducing consumption or preventing the energy depletion of batteries. Moreover, WPT, and in particular RF WPT, seems to be appealing for powering devices when environmental energy sources are not available or are intermittent [90]. Main concerns with RF WPT are the low efficiencies and safety issues related to the radiation power. The former is because since the power attenuation of the RF signal increases with the distance following a power-law, but also because of the shadowing and mutipath fading. The latter encloses established limits for transmit power in areas with presence of living beings, since the exposure to high levels of radiation might be harmful for the health [91, 92].

Conventional wireless sensor networks (WSN) consists of information access points (AP) and large number of sensors or other battery-driven end devices. In conventional WSN scenarios, only information is exchanged between nodes and information APs which leads to an eventual battery depletion, and hence, all the logistic issues previously discussed. An example of a conventional network is shown in Figure 4 (left). A solution to these problems would be to transform these setups into scenarios where the principles of RF wireless powered communications (WPC) are applied. To do this, information APs must be converted to hybrid access points (HAP) such that they transmit not only information but also power signals. It is also possible to place power beacons (PB) within the network, dedicated only to transmit energy while keeping the information APs and HAPs [93]. On the other hand, at the receivers side, the devices must incorporate the necessary hardware for EH, say, rectenna, splitter, etc. Figure 4 (right) shows a scenario with the mentioned modifications. A typical issue in scenarios similar to this one is the double near-far problem [56]. This problem arises when the PB/HAP broadcasts energy signals to devices that are indistinctly in the near and far region, or generates single energy beams using multiple antennas. On the one hand, devices close to energy sources harvest more energy and require less energy for transmission. On the other hand, those devices in the far region harvest less energy and require much more power to transmit. This unfairness among devices can be properly addressed by generating multiple beams at the transmitter (one for each device) or deploying mobile vehicles, for instance, unmanned aerial vehicles that can transfer energy to devices far from the HAP/PBs. However, the latter is only applicable to networks that are not delay-constrained due to the required time for the mobile vehicle to reach the device location. The scenario with both information and energy transfer consists of links operating in different ways, for example, nodes only harvesting energy, harvesting energy and decoding information simultaneously, and others that harvest energy and then transmit information. These distinct operation modes are enclosed into three canonical models for wireless information and energy transfer, WPT in the DL, wireless powered communication networks (WPCN) and simultaneous wireless information and power transfer (SWIPT) [56].

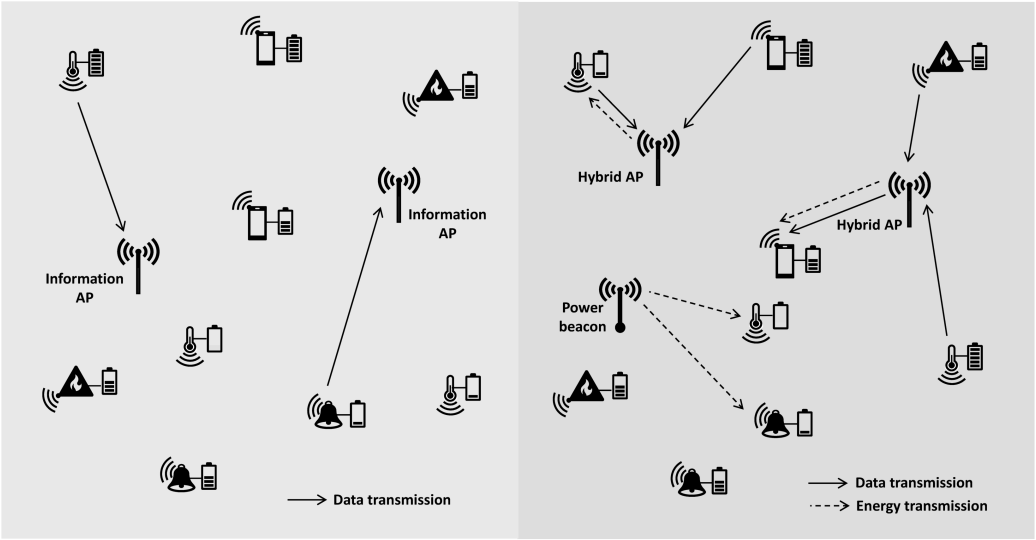

Figure 4. Typical WSN deployment. WSN with information transmission (left). WSN with information and energy transfer (right).

2.2.1 Wireless power transfer in the downlink

WPT has been historically thought for powering small form-factor devices over long distances. However, within the context of the IoT era, this idea has been reformulated to consider powering devices at moderate to short distances in the DL channel. The energy transfer must be as efficient as possible, and depends on the conversion efficiency at transmitter and receiver, and the transmission efficiency of the communication channel. The first two are closely related to hardware design, e.g., receiver rectenna design and transmit waveform optimization approaches, while the communication channel is optimized by applying more complex techniques than mere omnidirectional broadcasting. Precoding at the transmitter represents an efficient technique for improving the transmission efficiency in the channel, however, the CSI acquisition becomes a major issue since classical methods require feedback from the receiver which is not always a suitable strategy for energy-constrained devices. Let's comment first on the case of a MIMO channel with single user in the downlink. If we consider an energy transmitter (ET) device and an energy receiver (ER), both with multiple antennas, a good strategy for maximum energy transfer would be to transmit over the eigenvectors that correspond to the strongest eigenvalues of the channel matrix, exploiting spatial diversity, as in [94], where it is combined with frequency diversity. However, this strategy requires perfect CSI at the ET and then, optimal solutions for the acquisition are required. Although CSI is necessary at the ET under this strategy, other approach using CSI at the ER has also been considered using multiple antennas and performing combining at the RF stage, offering gains over DC combining [95]. The signal processing capabilities and hardware complexity of the ERs must be low, diminishing the energy consumption and assisting the CSI acquisition if required. Hence, ERs must have one block for communication (Cx) and another for EH [96]. These blocks utilize simultaneously the set of receive antennas (shared architecture) or utilize different antennas for their functioning (separate architecture), which are shown in Figure 5 [94]. The former allows easy CSI estimation,

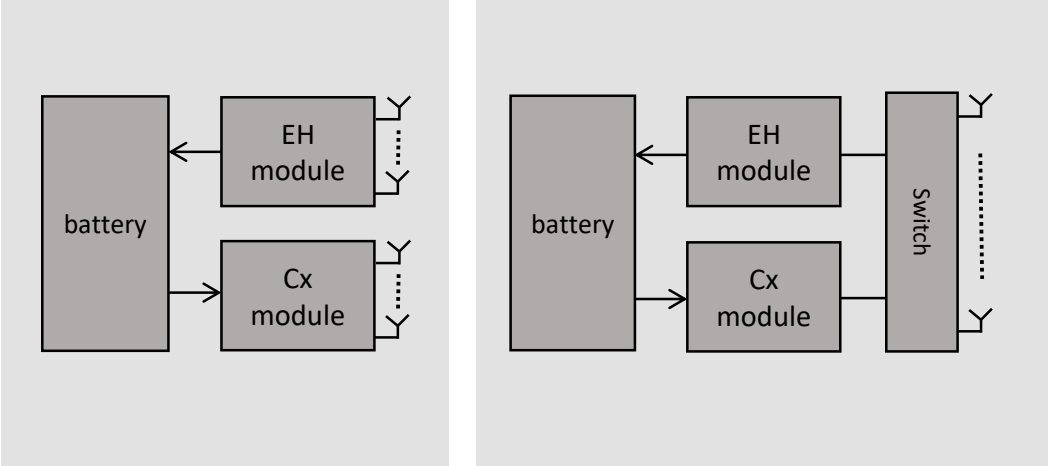

Figure 5. Antenna architectures for WPT. Separate-antenna (left) and shared-antenna (right) architectures.

smaller form-factor receivers, and EH and communication in time-division manner. The latter complicates the CSI estimation since the antennas for communication and for EH are not in the same position, hence the channel conditions are not the same. Let's comments now on some strategies for CSI acquisition.

- **Forward-link training with CSI feedback.** Techniques based on feedback from the receiver are common for the CSI estimation. In these setups, ETs transmit pilot signals to ERs for channel estimation and then receive feedback that allows energy beaming in the next phase. A common approach is to use the same frequency in both training and feedback stages in order to guarantee a proper estimation since the channel may be frequency selective [94]. Several works have been conducted in this area, for instance [96–99]. In [96], an adaptive beamforming using instantaneous CSI was proposed to maximize the harvested energy. In order to acquire the CSI at the transmitter, authors proposed a CSI quantization feedback strategy for maximizing energy and improving information decoding. In [97], authors derived the optimal power allocation for a multiple-input single-output (MISO) in a preamble-based training scheme with feedback from the receiver. They maximized the net harvested energy at the ER for fixed and variable preamble length and proved that with optimal power allocation the harvested energy with fixed length approaches the harvested energy with variable length, thus allowing lower complexity in the implementation. In [98], a scenario with limited feedback is studied, where information and energy receivers feed back bits for the quantized channel information based on random vector quantization. Moreover, they proposed a joint beamforming algorithm for scenarios with multiuser wireless information and power transfer. Finally, authors in [99] proposed an energy beamforming strategy that only requires partial CSI at the ET and reduces the feedback overhead for mobile stations when using joint wireless information and energy transfer. Schemes based on training with CSI feedback are applicable to setups with shared-antenna architecture but it is not suitable for scenarios where

the number of antennas to train at the ET is large (massive MIMO) due to time constraints.

- **Reverse-link training using channel reciprocity.** This technique strictly relies on the channel reciprocity properties, which in practice is difficult to achieve since requires precise calibration at both transmitter and receiver. Under this scheme, a fraction of the coherence time is used for sending the pilots to the ET, while feedback is not needed. Moreover, it is more efficient if compared to the previous method since it is suitable for large antenna arrays as the training overhead does not depend on the number of antennas at transmitter side. It also allows simpler architectures and less processing at ERs since CSI estimation is not required at that side of the network. Some trade-offs related to the training must be considered when implementing this approach, if the training duration is short, then, the CSI estimation would not be accurate, leading to a poor beamforming gain. On the other hand, if we practice excessive training, the energy consumption at the ER would be high while leaving less time for EH [94]. It is worth mentioning that this method is applicable to antenna-shared architectures since the channel must be the same in both directions. For instance, the authors in [89] studied a point-to-point MIMO channel exploiting channel reciprocity under Rician fading. They also proposed a framework in order to maximize the net harvested energy at the ER, considering the time and energy cost for the training.

- **Power-Probing with Energy Feedback**. One of the most popular approaches is the so-called energy beamforming with one bit feedback, discussed in [100]. It is applicable to setups with multiple ERs using separate antenna architecture. It basically consists in sending energy signals to the ERs, which then measure the harvested energy and send a feedback that considers past measurements. This allows the ET to adjust the energy signals depending on the received feedback. One bit of information for the feedback might be enough for the ET to know if the current transmission increased or decreased the harvested energy with respect to previous intervals, and update its strategy accordingly. Some other works have studied similar approaches. For instance, the authors in [101] proposed a simple method for the estimation of the CSI in a multi-antenna single-user system with WPT. They defined a codebook at the ET defined by Cramer-Rao lower bound analysis and used it as beamforming vector for transmission. Feedback for each vector is received using a signal strength indicator, the channel is then estimated via maximum likelihood analysis. Results proved the efficiency and simplicity of the proposed method. In [102], a multiuser MIMO system with WPT was studied. The authors presented a low-complexity scheme for efficiently power the devices in the DL channel where the ERs simultaneously send a common beacon signal and the ET conjugates and amplifies the sum of all signals in the WPT phase. Here, the double near far problem was solved by the use of an algorithm where the ERs adjust their beacons based on the amount of harvested energy.

These methods of CSI acquisition are usually valid in multi-user networks with energy multicasting. At this point it is worth commenting about the different multi-user network topologies in WPT and their pros and cons. The network architectures are enclosed within three major groups: coordinated multi-point WPT, locally-coordinated WPT and single ET WPT [94].

- **Coordinated multi-point WPT:** This is the case of a network with multiple ETs and ERs, where ETs jointly design the energy signals based on global CSI of all links. One of the main drawbacks is that in order to acquire that global CSI all ETs must be interconnected via backhaul to a central unit in charge of synchronization, signal optimization, etc.

- **Locally-coordinated WPT:** Under this approach cooperation is a key enabler since ETs must cooperate for an optimized functioning. For instance, the set of ETs could be grouped into clusters, each cluster serving a subset of all ERs. Other possible approach is to associate each ER to a subset of ETs depending on criteria such as distance or specific service, etc.

- **Single ET WPT:** This is the simplest case of a network architecture since each ER is associated to an specific ET depending in the channel state or other possible metrics. The main advantage over the previous two cases is that cooperation among ET is not required.

2.2.2 Wireless powered communication networks

WPCN refers to networks with information APs, HAPs, PBs and end devices, where energy is transmitted in the DL and information the UL channel as shown in Figure 4. The design of such networks must consider key trade-offs between DL energy and UL information rate, which we analyze herein. Since the principle behind WPCN is to power devices in the DL channel such that they harvest enough energy for the UL information transmission, efficient protocols must be designed, which is the case of the harvest-then-transmit protocol. This protocol is useful for both single user and multiple user networks and consists of two phases. In the first phase of duration τ_0T energy is transmitted in the DL, in this time the end devices harvest energy from the received signals and use it in the second phase of duration $(1-\tau_0)$T for information transition. The access in the UL occurs either in time-division or spatial-division multiplex access (TDMA and SDMA, respectively), although non-orthogonal multiple access (NOMA) techniques have been also studied recently. In the TDMA approach, the communication block is divided in K time slots τ_0T, τ_1T,...,τ_KT where $\sum_{i=0}^{K}\tau_i = 1$ and T is the block duration. Hence, the HAP/PB broadcasts energy in τ_0, while in each of the remaining time slots the devices transmit in the UL channel. This approach was investigated in [103] where the authors maximized the sum throughput of all users in the network by finding the optimal values for τ_i for each user in a network powered by an HAP. The solution for maximum throughput was to allocate more time to the users close to the HAP and less time to those far away, creating certain unfairness in the network. This problem arose due to the presence of the previously commented double near far problem. The solution was to introduce an additional constraint to the optimization problem limiting the rate of each user to a minimum value. The solution showed more fairness among users at the penalty of smaller sum throughput. In [104] authors studied the energy consumption and SE of TDMA based WPCN and NOMA based WPCN and derived expressions for them. As result, they proved that TDMA based approach is both more energy and spectral efficient. NOMA and TDMA approaches were also sudied in [105], and in addition to the derivation of the optimal values of τ, authors also proved that TDMA is more

efficient than NOMA when the circuit power consumption is non-negligible. The other access method in the UL is SDMA, which relies on the capabilities of array antennas to decode the incoming signals. Instead of transmitting just in a portion of time, the end devices can transmit continuously, thus improving the SE. The work in [106] considered a scenario with an HAP with multiple antennas and multiple single-antenna end devices with energy beamforming in the DL and SDMA access in the UL channel. In order to achieve fairness, the minimum throughput within the network was maximized by a jointly design of UL and DL time allocations. The sum EE of users was maximized in [107] by jointly optimizing the users transmit power, beamforming and time allocation for TDMA and SDMA in the UL. The authors also proved that the scheme with SDMA outperforms TDMA when the throughput requirement is high.

WPCN also involve other criteria for the design that modify the performance if considered. The location of information and energy sources play a key role, these sources can be co-located or separated in the scenario. Moreover, the communication can be HD or FD, depending on the hardware availability. If FD is used, SIC techniques are required at the transmitter side if co-located architecture is implemented, while sER is an attractive option at the receiver for better EE. These considerations were studied in [108], where the users' weighted sum rate was maximized by optimizing the time allocation for each user and transmit power in a scenario with an HAP and multiple users operating in FD mode. Furthermore, the same problem was presented for the HD case. Results showed that the scheme operating in FD outperforms the scheme with HD when SIC is good enough.

2.2.3 Simultaneous wireless information and power transfer

Other approach for powering energy constrained communication devices is SWIPT. This schemes aims at sending both information and power in the DL channel using the same RF signal, i.e., receivers must collect energy and decode the information carried by the incoming RF waves. Hence, the optimization of the receiver architectures is critical in order to achieve a balanced performance between EH and communication rates. Some receiver architectures have been proposed in the literature for SWIPT, which we cover herein. First of all, it is worth pointing out that such architectures are for co-located placement of the information decoding and EH. Moreover, the operation principles of EH and information reception impose different requirements for correct operation, such is the case of the signal sensitivities, where the values for information reception can be very low as long as they are still high compared to the noise level (high SNR), while the sensitivities for EH are much higher due to the energy requirements and hardware impairments.

The first architecture is known as power splitting (PS), where the power of the incoming signal plus antenna noise power is divided using a power splitter (see Figure 6 a)) by a ratio ρ for EH and $1-\rho$ for information decoding. The division is done before information reception and EH since energy cannot be harvested after information decoding and vice versa. In PS, it is possible to use a fixed value of ρ but the optimal solution is the use of a value that changes over time. This is because in the presence of fading the communication channel varies over time and, under poor channel conditions, might lead to smaller values of ρ, which are desirable to favor information decoding, and vice versa. Time switching

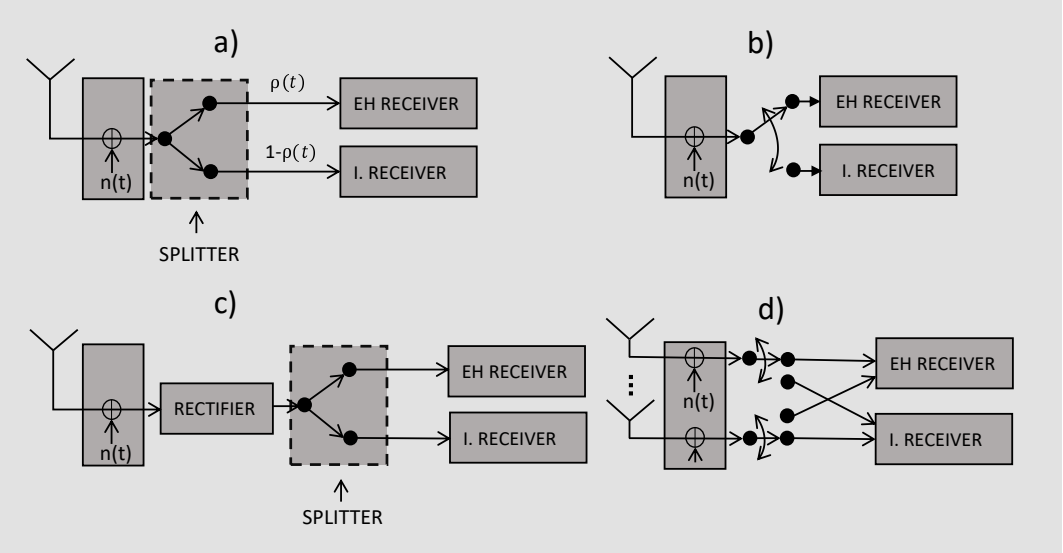

Figure 6. Receiver architectures SWIPT.

(TS) is another option for simultaneous EH and information decoding (see Figure 6 b)) where a group of symbols is used for EH and the rest for information reception. The performance of this scheme is worst than that of the PS approach since not all the time is used for information decoding, hence, the achievable communication rates are lower. These two schemes PS and TS are discussed in [109], where authors proposed an ON-OFF PS which is a combination of TS and dynamic PS and an integrated architecture for both energy harvesting and information decoding. They derived optimal transmission strategies for different energy-rate trade-offs. The integrated architecture is shown in Figure 6 c), and notice that it introduces a rectifying circuit before PS, which eliminates the phase of the signals, hence, it is only suitable for energy modulation strategies and it is more inefficient from the SE point of view due to the elimination of degrees of freedom. All these schemes must consider the energy spent on the processing circuits, whose consumption represents the higher part of all spent energy. The last architecture for energy receivers is known as antenna switching (AS) (see Figure 6 d)), which provides lower hardware complexity. In this scheme, a subset of the total number of antennas is used for EH while the rest for information decoding and it is defined as a low-complexity implementation of PS. The main difference with respect to PS is that each antenna can be directly connected to either the information decoding or EH blocks [56]. The work in [110] formulated a resource allocation problem to maximize the network energy efficiency in a scenario where a cooperative scheme with SWIPT was proposed. The proposed protocol consisted of conflict-free schedule initialization, cooperative resource allocation and heuristic algorithms to obtain the transmission policy with maximum EE. The work in [111] maximized the sum UL and DL rates by optimizing time, subcarrier and power allocations in a scenario with OFDM and SWIPT in the DL channel. On the other hand, authors in [112] investigated joint power allocation and TS control for EE optimization in a scenario with NOMA and SWIPT. They proved that the combination of NOMA and SWIPT achieves significant gains with respect to classical orthogonal access systems in terms of EE.

2.2.4 Self-energy recycling

sER has been proposed to improve the EE, allowing to reuse part of the energy spent on transmission. In Section 1.2, possible strategies to improve EE were discussed, mentioning EH as a promising EE-enabler. We can consider sER as a variant of EH which is able to provide significant levels of recycled energy, mainly in devices with considerably high transmission powers where the antennas for recycling are close to transmit antennas, hence, suitable to improve the EE at BSs. However, this technique can be also exploited in devices with small form-factor and lower energy consumption in transmission. Although sER has been considerably investigated, e.g., [113–118], there are still open problems for extensive research. In [113], the authors studied an FD relay network operating under the amplify-and-forward (AF) protocol where the relay node receives dedicated power signals for EH and perform sER when transmitting the data to the destination node. The setup was proposed with MISO architecture achieving considerable gains in terms of throughput with uninterrupted information transmission. The work in [114] studied an AF relay cooperative network, where the beamforming vector is optimized for maximum rate considering sER. Results showed that the scheme using sER outperforms time-switching (TS) and power-splitting (PS) relay protocols. In [116], the authors investigated a sER powered multiantenna relay channel for coverage extension either in small cells or WSNs. They proposed an optimal beamforming for DL only and, both UL and DL channels. It was also proved that high values of sER improve the performance of conventional relay networks. In [115], the secrecy rate is maximized by jointly optimizing energy and beamforming vectors. Therein, the network consisted of an energy source, an FD information source with sER, an information receiver and a potential eavesdropper. [117] studied an FD point-to-point network with a multi-antenna AP and a mobile receiver with two antennas where SWIPT is assumed and sER is performed at the receiver. Authors jointly designed beamforming vector for transmission, PS ratio and transmit power for minimizing the sum transmit power. In [118], a scheme with a BS serving an UL and a DL device under quasi-static Rayleigh fading is presented. The authors determined the optimal portion of the communication block for sER and the optimal value of power delivered by the source for maximizing the EE.

2.3 Diversity as enabler for URC

Any application within the category of URC requires considerable high SNR levels in reception so that the signal is decoded without errors. Communication systems that transmit and receive using simple schemes are more exposed to errors since the signal is likely to suffer deep fades, which significantly deteriorates the performance. However, this phenomenon is avoidable to some extent with the use of diversity techniques. These techniques are mainly grouped within three categories, time diversity, frequency diversity and spatial diversity. We will comment on them, although the focus will be mainly on the case of spatial diversity.

2.3.1 Time diversity

Diversity over time is attainable by transmitting the same signal at different times. However, this is not suitable if the channel coherence time is infinite (stationary applications) since the fading is correlated over time. This technique is also attainable by the use of coding and interleaving, i.e., the signal is coded and then consecutive symbols are transmitted over different coherence intervals so that errors are spread over several codewords, which is useful against the occurrence of burst errors. One of the simplest forms of time diversity is retransmission, where the transmit node sends the same information several times, with our without feedback from the receiver [119]. The use of coding must be considerable analyzed since it carries a series of trade-offs which are critical for certain applications. For instance, its use brings a coding gain defined as the difference in SNR of schemes with and without coding for similar probability of error, however, such gain may be negative if the operation is in the low SNR regime, which is not desirable in any case. The use of coding for time diversity also implies a rate penalty or bandwidth increase, being a constraint for certain applications requiring a minimum bitrate or with a fix available bandwidth. Nevertheless, these issues can be addressed with the use of Trellis codes [120, 121]. Time diversity improves the reliability in a communication system since the probability of errors is reduced due to redundancy over time, retransmissions, coding and interleaving, but might not be suitable for delay constrained applications where the latency requirements are strict.

2.3.2 Frequency diversity

Frequency diversity is another alternative when the communication system imposes certain reliability requirements. The main principle is to send the same signal through different carrier frequencies separated at least by the coherence bandwidth of the channel, and it is applicable for frequency selective channels [120, 121]. Moreover, frequency diversity is not suitable for systems where the available spectrum is limited. Frequency hopping spread spectrum mechanism is an example of frequency diversity, where several frequencies are used for the communication. Frequency hopping in the medium access control (MAC) layer is implemented through the use of different frequencies in each communication stage between devices, i.e., the nodes communicate at a certain frequency in a time instant and change to another frequency in the following one [122]. The impact of frequency diversity in the multipath fading has been the center of discussion in several works, e.g., [123–125]. The authors in [123] proved that the effect of fading is reduced by the use of frequency hopping, while in [124] such benefit is also reached by the use of adaptive routing techniques. Moreover, the combined use of adaptive routing and frequency hopping was studied in [125] for delay constrained applications.

2.3.3 Spatial diversity

The main idea behind diversity techniques is to create multiple paths of the transmit signal so that the fading is uncorrelated over each of them. We have seen so far that these uncorrelated paths can be achieved using time and frequency diversity, nevertheless, these

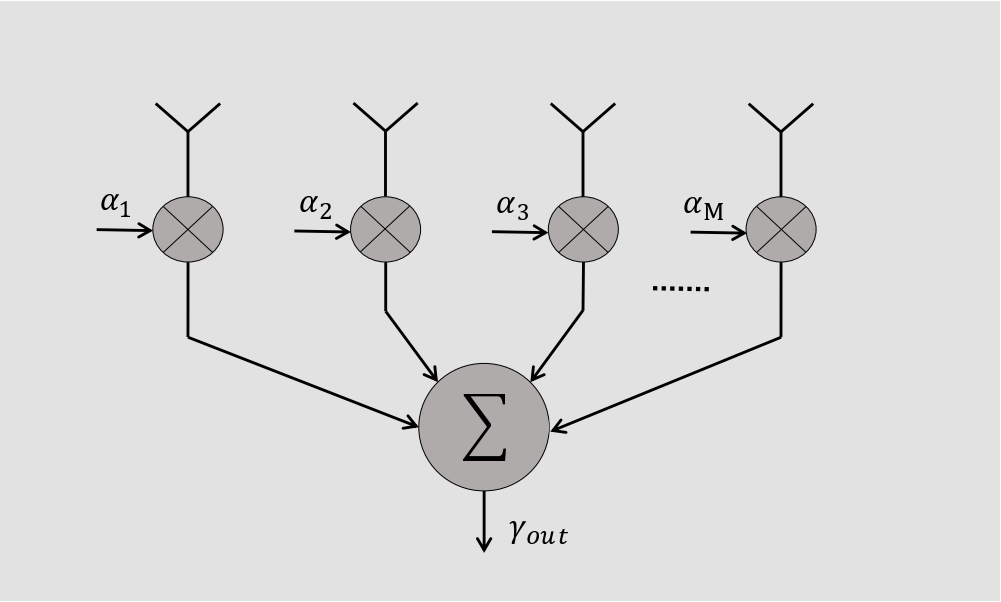

Figure 7. Generic combiner for spatial diversity at the receiver side.

are not the only options. Spatial diversity, also known as antenna diversity has become one of the most popular and practical diversity schemes for achieving ultra-reliability in communications systems. It is divided in transmit and receive diversity depending on the side of the network where it is applied. As the name suggests, multiple antennas are used and placed at certain distances from each other so that correlation among the transmit/receive signals is minimized. This is important since closely placed antennas leads to signals experiencing similar channel behaviour, thus reducing the benefits from diversity. When using spatial diversity, the amplitude and phase of the transmit/receive signals are usually manipulated with the goal of maximizing the net SNR, and hence, reducing the probability of error when decoding the signal. An important advantage is that these approaches can be implemented without extra bandwidth or signal power [120, 121].

We will shortly comment on the most common spatial diversity schemes found in the literature, which are selection combining (SC), threshold combining, maximal ratio combining (MRC) and equal gain combining (EGC) at the receiver side, and maximal ratio transmission (MRT) at the transmitter side. Finally we cover MIMO systems and some practical considerations. Figure 7 shows the general structure of a receive combiner, which we use as reference for all schemes [121]. It represents a linear combiner with M branches, each branch has an antenna and a block where the signal is weighted by a factor α_i which considers the phase and amplitude of the incoming signals. Moreover, the signals are added up at the block $\sum$ providing an output with SNR γ_{out}.

- **Selection combining:** This scheme selects the branch with the highest SNR and outputs its signal. In SC, a single branch is active at a time, hence, a single receiver is required. However, if the node is constantly receiving information the use of several receivers is required for sensing all the SNRs in the branches. The output SNR under this approach is $\gamma_{out} = \arg \max \gamma_i$ with $i \in [1, 2, ..., \mathrm{M}]$. Reliability with SC has been investigated in [126], where the performance of transmission of

small data over fading channels is analyzed. The authors derived expressions for the delay outage probability under diverse schemes and proved that the use of rate-adaptive transmission with SC fulfills the latency and reliability requirements for IoT applications. On the other hand, expressions for minimum duration outages were derived in [127] under Rayleigh fading with SC. The proposed expressions proved to be accurate withing fading margins of 0 to 10 dB. SC improves the reliability if compared to a single antenna system since the highest SNR branch is always used for decoding. When the number of branches increases, the outage probability decreases since it is more likely to have branches with high SNRs. However, the performance of SC might not be comparable to other schemes as we further discuss.

- **Threshold combining:** A simpler criterion to SC is the so-called threshold combining. As the name suggests a given SNR threshold is selected for the operation. With this scheme, instead of using M receivers for constant sensing, one single receiver is used, therefore, a single branch is active at a time. A branch is initially chosen, and if the SNR is above the threshold, then the same branch remains active. However, when the SNR falls below the target the receiver is switched to another branch until the SNR is above the threshold. If the number of branches is two, the scheme is known as switch and stay combining (SSC). The branch selection could be random or following an specific order or pattern. Some other variants of this scheme have been proposed, for example, the authors in [128] presented a protocol called distributed secure switch-and-stay combining (DSSSC) in order to reduce the complexity of a DF network while keeping secure performance (secrecy outage probability) in the presence of an eavesdropper. For ultra-reliability SSC was studied in [129], serving an IoT device with a single RF chain. Under this scheme it was proved that SSC outperforms SC in terms of average error probabilities when choosing the optimal threshold value.

- **Maximal ratio combining:** This scheme is one of the most popular when implementing receive diversity. Different from previous schemes where the output is the SNR of one of the branches, in MRC the output is a weighted sum of the SNR of all branches. Clearly, more weight must be given to those branches with higher SNR. Not only the amplitude is considered in MRC but the phase of the incoming signals, this is under the principle of constructive addition such that the output SNR is maximized [121]. The knowledge of the CSI is mandatory under this scheme for optimum performance since imperfect or no CSI at the receiver causes no alignment between combining vector (vector which contains all coefficients α_i) and incoming signals. In [130], authors studied the performance of two grant-free schemes with shared resources with MRC at the receiver in Rayleigh fading. They showed the benefits of using larger number of antennas at reception in terms of outage probability under a stop-and-wait protocol with scheduled retransmissions. In [131], the authors compared the performance of physical layer abstraction methods for multiconnectivity orthogonal frequency division multiplexing (OFDM) based in terms of minimum mean square error. They proved that for higher diversity orders with MRC, the performance of physical layer abstraction methods increases. The superiority of MRC over SC in terms of EE with an optimal power control and rate allocation scheme was proved in [132] with stringent reliability requirements.

However, for large number of antennas, SSC was proved to be more energy efficient than MRC.

- **Equal-gain combining:** This scheme simplifies the complexity introduced in MRC due to the requirements of CSI availability. EGC co-phases the signal on each branch and applies a similar weight to all of them. The penalty to be paid according to [121] is less than 1 dB of power.

- **Maximal ratio transmission:** This spatial diversity approach is applied at the transmitter side where multiple antennas are used in order to create multiple paths in the communication channel. Different weights are applied to each branch and the phase is adjusted using a precoding vector so that all paths add up constructively at the receiver. The knowledge of the channel is also compulsory for optimum performance. The absence of instantaneous CSI would lead to the use of fixed weights and phases or channel statistics [133] (for instance, matrix covariance matrix) which is not optimal for maximum SNR, and hence, higher error/outage probabilities [120]. [134] studied the outage probabilities for a multi-antenna system using MRT. Therein, authors proposed a modified MRT scheme with precoding vector considering the power constraints at each antenna. Results showed that the modified MRT performs better than classical MRT schemes in terms of outage probability. In [135], the optimal resource allocation for MISO broadband orthogonal frequency division multiplex access (OFDMA) was investigated. The resource allocation was investigated through the solution of a non-convex optimization problem for maximizing the system throughput. Results showed that the use of multiple antennas at the BS with MRT improves reliability and latency.

- **MIMO systems:** We have focused so far in spatial diversity at either the transmitter or receiver. Such schemes are able to provide certain power and beamforming gains as in case of MRT and MRC, however, they were analyzed for scenarios with one single antenna at transmitter or receiver. In the case of MIMO systems, multiple antennas are used at both sides of the network, providing not only beamforming and power gains but also degrees-of-freedom gains, which are exploited by spatial multiplexing of several data streams onto the channel. The MIMO channel is characterized by a matrix with dimension M $\times$ N, where M and N represent the number of transmit and receive antennas, respectively. A common practice is to transmit and receive through the strongest eigenmodes[1] and to use the complex conjugate of the corresponding eigenvectors for precoding and combining. This allows not only improvements in reliability but also in capacity in rich scattering environments with low correlation among paths, where the rank of the channel matrix increases [120, 121]. Other technology that has been considered as an enabler for future networks is massive MIMO (mMIMO), which considers the use of a large amount of antennas for transmission/reception such that the transmit antennas outnumber users. mMIMO brings benefits in EE, SE and allows

[1]The term comes after applying the singular value decomposition to the MIMO matrix, where the original matrix is decomposed into three as $\mathcal{M}$=UΔV* with $\mathcal{M}$ as the original matrix, U and V* are matrices containing the corresponding eigenvectors and Δ is a diagonal matrix containing all the eigenvalues in decreasing order [120].

user tracking through very narrow beams created at the transmitter [136].
Ultra reliability has been closely linked to MIMO/mMIMO systems. For instance, the authors in [137] proposed a non-coherent mMIMO framework for enabling URLLC based on a multiuser space-time modulation scheme. They also jointly optimized the constellations of multiple users and proved that the optimized scheme considerably improves the reliability. On the other hand, the work in [138] presented the guidelines required for designing mMIMO systems under URLLC constraints in short packet transmission regime. They also proved that a BS with 100 antennas contributes to avoid pilot contamination and error probabilities below 10^{-5} are attainable using minimum mean square error (MMSE) in both UL and DL. In [139], a mMIMO system was analyzed in the presence of shadowing. Moreover, it was proved that reliability is attainable when the number of receive antennas is large with short packet transmission. Expressions for the error probabilities were derived with perfect and imperfect CSI with zero-forcing detection. Authors in [140] investigated the problem of URLLC in mMIMO systems operating with millimeter waves. They maximized the network utilization under strict reliability and latency requirements and proposed a utility delay-control scheme ensuring reliability and reducing latency.

2.4 Other related works

So far we have covered topics that are closely related to the present work. Now we cover some works that combined more than one of the previous concepts and keep certain similarity with our model. For example, the benefits of performing sER in an FD small base station (SBS) in terms of energy efficiency were studied in [141]. However, reliability was not considered neither the possible benefits of using sER in this regard. The work in [142] solved the problem of maximizing the throughput of the far user while maintaining the target throughput for near users. Authors assumed NOMA with imperfect SIC in a battery assisted RF-EH scenario. The work, however, only considered single antenna devices. In [143], the focus is on sER in FD relaying MIMO OFDM systems, where the SE was maximized and the optimal power allocation per antenna was derived. Therein, the network reliability was not considered. Authors in [144] evaluated an accumulate-then-transmit framework for multiuser scheduling in an FD wireless-powered system with multiple IoT devices powered via RF-EH and one FD HAP. The HAP operates in FD mode with a limited number of antennas. Furthermore, the benefits of sER were not exploited. On the other hand, the work in [145] analyzed a SWIPT system with IoT nodes operating in FD where the total transmit power is minimized via a jointly optimization of a hybrid precoder, decoding rule and PS ratio. The benefits of sER were not exploited while the number of antennas for transmission and reception was constant. Finally, authors in [146] minimized the system outage probability in the presence of an FD DF EH relay by properly tuning the PS factor. The devices were assumed with single antennas and sER was not considered. It is worth mentioning that these works assume that the energy is only consumed on transmission, ignoring the hardware energy consumption.

3 HD AND FD SCHEMES WITH SELF-ENERGY RECYCLING-AIDED RELIABILITY

In this chapter, we present the system model for two scenarios with HD and FD communications, derive expressions for the outage probabilities in all cases considering the impact of sER in the performance, and present the proposal for minimizing the outage probability of the worst link.

3.1 System model

For the analysis, we consider an SBS which serves two devices, one in the DL channel and the other in the UL channel. The SBS is powered by a regular source that delivers $\mathrm{P_G}$ Watts at most. Moreover, the SBS is equipped with Q RF chains used for transmission ($\mathrm{T_x}$)/reception ($\mathrm{R_x}$) or both, and P antennas for sER. The devices operate at constant rates, r_{sbs} in the UL and r_d in the DL. Furthermore, we assume quasi-static Rayleigh fading in both links, i.e., the channel coefficients remain constant over the duration of a time block T and change independently from one block to another. We also consider the use of spatial diversity, in this case MRC in the UL and MRT in the DL. Full CSI is assumed at the SBS, which is a common approach when precoding and combining techniques are implemented [147].

Here we define symbols and operators which are used in the following sections. $||\cdot||$ represents the norm operator and $(\cdot)^T$ is the transpose operation. Moreover, the $(\cdot)^H$ denotes the Hermitian operation in vector notation. $\Gamma(\cdot)$ denotes the upper incomplete gamma function and gamma distribution, and ${}_1F_1(\cdot)$ the confluent hypergeometric function of first kind [148, Eq.(13.2.2)]. The terms $\beta(\cdot)$ and ${}_2F_1(\cdot)$ represent the beta function and the Gauss hypergeometric function [148, Eq.(15.2.1)], respectively.

3.2 Half-duplex mode

The first scheme considers a SBS that operates in HD mode. The SBS uses M antennas for both transmission and reception such that $\mathrm{M} = \mathrm{Q} \geq 2$, and $\mathrm{P} \geq 0$ antennas for sER ($\mathrm{P} = 0$ means no sER). Figure 8 shows the mentioned setup, here, TD and UR denote the links $\mathrm{T_x} \rightarrow D$ and $U \rightarrow \mathrm{R_x}$, respectively. As in all HD schemes, the communication is divided into two phases. In the first part of duration, τT ($\tau \in [0, 1]$) where T is the overall communication time, the SBS transmits information to D using MRT with precoding vector $\mathbf{w}_{\mathrm{td}} = \mathbf{h}_{\mathrm{td}}/||\mathbf{h}_{\mathrm{td}}||$ [120], where $\mathbf{h}_{\mathrm{td}} = [\mathrm{h}_1, \mathrm{h}_2, ..., \mathrm{h}_\mathrm{M}]^T$ is a column vector containing all the zero-mean unit-variance complex Gaussian channel coefficients between the SBS and D. In this communication phase, U remains inactive and sER is performed at the set of P antennas. In the second part of duration $(1-\tau)$T, U starts transmitting and the SBS switches to reception mode applying MRC to the received signal with combining vector $\mathbf{w}_{\mathrm{ur}} = \mathbf{h}_{\mathrm{ur}}/||\mathbf{h}_{\mathrm{ur}}||$, where $\mathbf{h}_{\mathrm{ur}} = [\mathrm{h}_1, \mathrm{h}_2, ..., \mathrm{h}_\mathrm{M}]^T$ is a column vector that contains the channel coefficients between U and the SBS, following the same distribution as $\mathbf{h}_{\mathrm{td}}$.

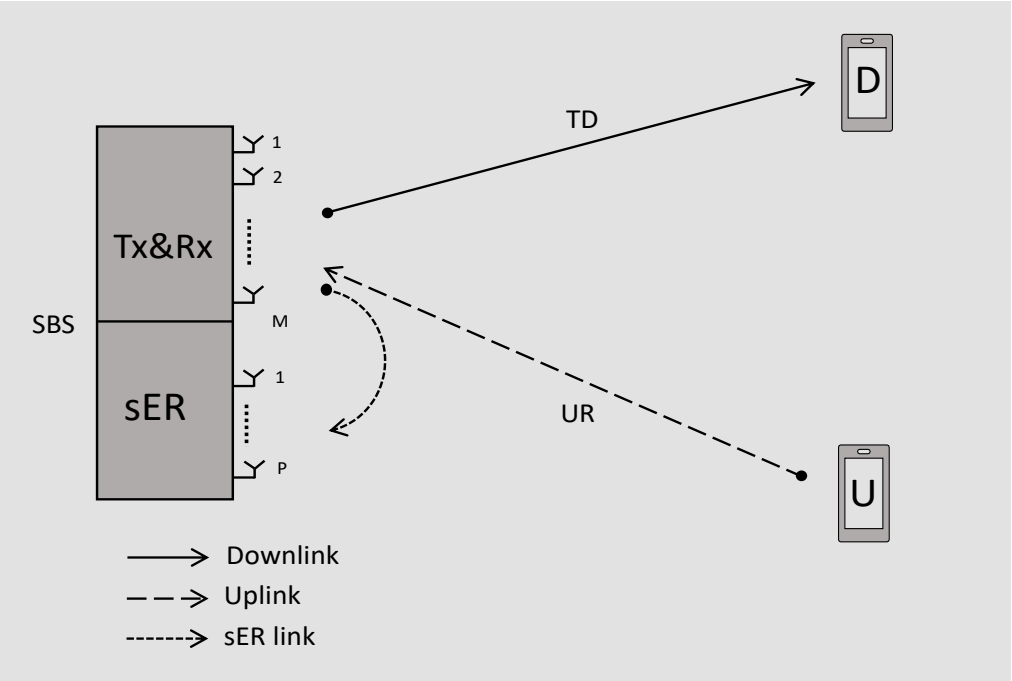

Figure 8. HD sheme. The SBS communicates with U and D via UL and DL channels, respectively.

3.2.1 Signal model

The signal received at D in the first phase is expressed as follow

$$\mathrm{y_d} = \sqrt{\varphi_{td}(P_{\mathrm{EH}} + P_{\mathrm{RF}})}\mathbf{w}_{\mathrm{td}}^{H}\mathbf{h}_{\mathrm{td}}s_s + n_{\mathrm{d}} = \sqrt{\varphi_{\mathrm{td}}(P_{\mathrm{EH}} + P_{\mathrm{RF}})}||\mathbf{h}_{\mathrm{td}}||s_s + n_{\mathrm{d}}, \tag{1}$$

where φ_{td} represents the path gain in the link (path gain = path loss^{-1}), $\mathrm{P_{EH}}$ is the power obtained from the sER process, $\mathrm{P_G}$ is the power received from the source, s_s represents the baseband transmitted signal such that its expected value is $E\{|s_s|^2\} = 1$, and n_{d} represents the additive white Gaussian noise (AWGN) with zero mean and variance σ^2. It is worth mentioning that in practice all the power delivered by the source is not converted and transmitted, instead, part of the power is dissipated in the active elements present in the RF chains (power amplifiers, mixers, etc). For now, we consider the ideal case where $\mathrm{P_{RF}} = \mathrm{P_G}$, but in later analysis we introduce a more realistic approach. With the expression of the signal at D, we can obtain the SNR as

$$\gamma_{\mathrm{d}} = \frac{|\sqrt{\varphi_{td}(\mathrm{P_{EH}} + \mathrm{P_{RF}})}\mathbf{w}_{\mathrm{td}}^{H}\mathbf{h}_{\mathrm{td}}s_s|^2}{\sigma^2} = \frac{\varphi_{\mathrm{td}}(\mathrm{P_{EH}} + \mathrm{P_{RF}})||\mathbf{h}_{\mathrm{td}}||^2}{\sigma^2}, \tag{2}$$

where $||\mathrm{h_{td}}||^2 \sim \Gamma(M, 1)$ since it represents the sum of M unit-mean exponential random variables (RVs), i.e, the distribution of the power of Rayleigh fading is exponential and the sum of exponential RVs follows a gamma distribution.

In the second phase of communication, the SBS receives the signal from U and stops the sER/EH process, this is because the received signal is typically in the order of μW

which is useful for information decoding but not for EH since the SBS consumes higher power levels. The signal at the SBS is given by

$$\mathrm{y}_{\mathrm{sbs}} = \sqrt{\varphi_{\mathrm{ur}}\mathrm{P}_{\mathrm{u}}}\mathbf{w}_{\mathrm{ur}}^{H}\mathbf{h}_{\mathrm{ur}}s_{\mathrm{u}} + \mathbf{w}_{\mathrm{ur}}^{H}\mathbf{n}_{\mathrm{s}}, \tag{3}$$

where φ_{ur} represents the path gain in UR, P_{u} depicts the transmit power at U, s_{u} is the baseband transmitted signal such with expected value $E\{|s_{\mathrm{u}}|^2\} = 1$, and $\mathbf{n}_{\mathrm{s}}$ represents the AWGN vector at the receive antennas with zero mean and variance σ^2. Similarly, we can derive the expression for the SNR at the SBS after MRC as

$$\gamma_{\mathrm{sbs}} = \frac{|\sqrt{\varphi_{\mathrm{ur}}\mathrm{P}_{\mathrm{u}}}\mathbf{w}_{\mathrm{ur}}^{H}\mathbf{h}_{\mathrm{ur}}s_{\mathrm{u}}|^2}{E\{|\mathbf{w}_{\mathrm{ur}}^{H}\mathbf{n}_{\mathrm{s}}|^2\}} = \frac{\varphi_{\mathrm{ur}}\mathrm{P}_{\mathrm{u}}|\mathbf{w}_{\mathrm{ur}}^{H}\mathbf{h}_{\mathrm{ur}}|^2}{||\mathbf{w}_{\mathrm{ur}}||^2\sigma^2} = \frac{\varphi_{\mathrm{ur}}\mathrm{P}_{\mathrm{u}}||\mathbf{h}_{\mathrm{ur}}||^2}{\sigma^2}, \tag{4}$$

where $||\mathbf{h}_{\mathrm{ur}}||^2 \sim \Gamma(M, 1)$. As previously mentioned, in the first phase the SBS performs sER using the set of P antennas and the associated conversion hardware. For maximum conversion efficiency, we assume the architecture proposed in [149], which contains antennas, phase shifting circuitry, charge pumps, a combiner and an energy storage, in that order. By using this scheme, we guarantee maximum conversion efficiency since the output direct current (DC) is the sum of all current streams generated by each branch. Figure 9 shows the adopted architecture for RF-DC conversion. Hence, following this model we can determine the harvested energy at the SBS. The RF signal at P is expressed as follows

$$\mathbf{y}_{\mathrm{p}} = \sqrt{\varphi_g(\mathrm{P}_{\mathrm{EH}} + \mathrm{P}_{\mathrm{RF}})}\mathbf{w}_{\mathrm{td}}^{H}\mathbf{G}s_s + \mathbf{n}_{\mathrm{p}}, \tag{5}$$

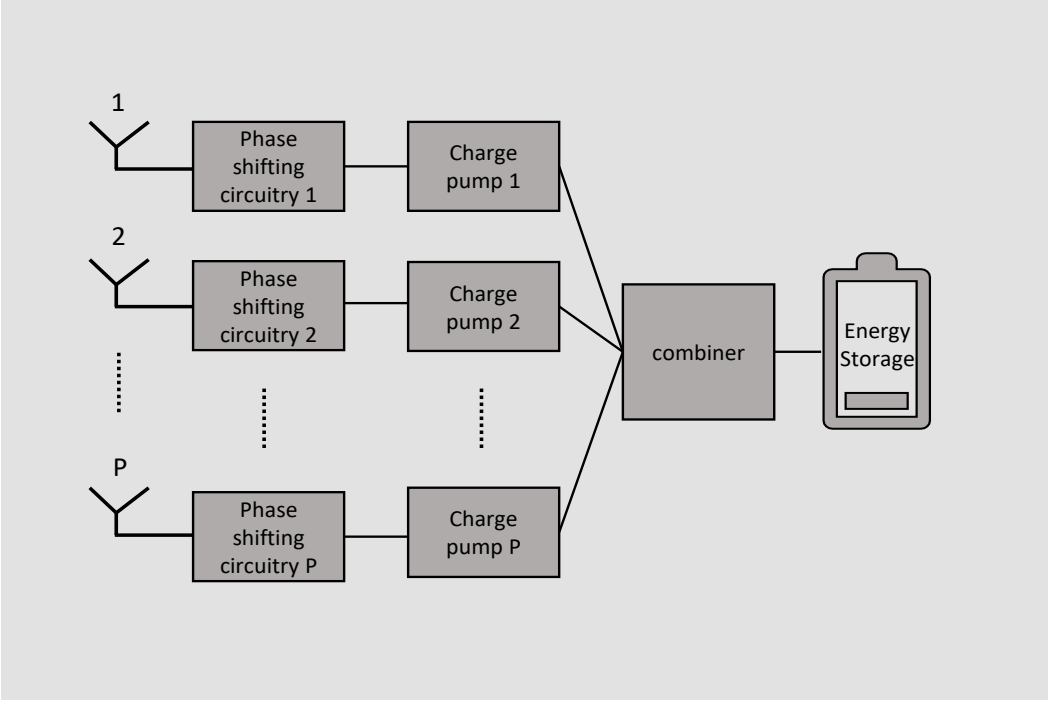

Figure 9. Architecture for maximum RF-DC conversion efficiency [149].

where φ_g represents the path gain in the link $\mathrm{T_x} \rightarrow$ sER, $\mathbf{G}$ is a $\mathrm{M} \times \mathrm{P}$ matrix containing all the channel coefficients between the M transmit and P sER antennas. We assume these channels equal and constant, since they more likely experience near field rather than far field properties [118], nevertheless, this depends on the antenna separation and λ. It is also possible to model these channels following a Rician distribution with high LOS factor, as previously mentioned in Section 2.1.1, making them quasi-deterministic. Now, the harvested energy is expressed as

$$\begin{aligned} E_{\mathrm{EH}} =& E_s\left\{\tau \mathrm{T}\eta\mathrm{P}\left|\sqrt{\varphi_g(\mathrm{P_{EH}}+\mathrm{P_{RF}})}\mathbf{w}_{\mathrm{td}}^H\mathbf{G}s_s\right|^2\right\}, \\ =& E_s\left\{\tau \mathrm{T}\eta\mathrm{P}\left|\sqrt{\varphi_g(\mathrm{P_{EH}}+\mathrm{P_{RF}})}\sum_{i=1}^{\mathrm{M}}\mathrm{w}_{\mathrm{td},i}gs_s\right|^2\right\}, \\ =& \tau \mathrm{T}\eta\mathrm{P}\varphi_g(\mathrm{P_{EH}}+\mathrm{P_{RF}})|g|^2\left|\sum_{i=1}^{\mathrm{M}}\mathrm{w}_{\mathrm{td},i}\right|^2. \end{aligned} \tag{6}$$

Here, the conversion efficiency $\eta \in (0,1)$ is introduced, where we assume the linear model for simplicity. Notice that the expectation is taken with respect s_s and the noise power was not considered for sER due to its low contribution. g represents the channel coefficients of matrix G and $\mathrm{w_{td,i}} = \mathrm{h_{td,i}}/||\mathbf{h_{td}}||$ depicts the individual values of the precoding vector. The expression in (6) represents the harvested energy in τT, now we can take it to the power domain dividing both sides of the equation by T, then we have

$$\mathrm{P_{EH}} = \tau\eta\mathrm{P}\varphi_g(\mathrm{P_{EH}}+\mathrm{P_{RF}})|g|^2\left|\sum_{i=1}^{\mathrm{M}}\mathrm{w}_{\mathrm{td},i}\right|^2. \tag{7}$$

Notice that the term $\mathrm{P_{EH}}$ is present in both sides of (7), which indicates the presence of an "*energy loop*". Therefore, we can isolate the term and obtain

$$\mathrm{P_{EH}} = \frac{\eta\mathrm{P}\varphi_g|g|^2\mathrm{P_{RF}}\left|\sum_{i=1}^{\mathrm{M}}\mathrm{w}_{\mathrm{td},i}\right|^2}{1-\tau\eta\mathrm{P}\varphi_g|g|^2\left|\sum_{i=1}^{\mathrm{M}}\mathrm{w}_{\mathrm{td},i}\right|^2}. \tag{8}$$

This expression holds provided that $\tau\eta\mathrm{P}\varphi_g|g|^2\left|\sum_{i=1}^{\mathrm{M}}\mathrm{w}_{\mathrm{td},i}\right|^2 < 1$ since the denominator cannot be negative, which is ensured due to $\tau, \eta < 1$ and the small values of φ_g.

3.2.2 Distribution of the harvested power

Note that $\mathrm{P_{EH}}$ is dependent on the term $\left|\sum_{i=1}^{\mathrm{M}}\mathrm{w}_{\mathrm{td},i}\right|^2$, which we denote as Z for ease of notation, then, $\mathrm{Z} = \left|\sum_{i=1}^{\mathrm{M}}\mathrm{w}_{\mathrm{td},i}\right|^2 = \frac{|\sum_{i=1}^{\mathrm{M}}h_{\mathrm{td},i}|^2}{||\mathbf{h}_{\mathrm{td}}||^2}$. We stated before that $||\mathbf{h}_{\mathrm{td}}||^2$ is gamma distributed. Moreover, the numerator of Z represents the sum of M zero-mean unit-variance Gaussian RVs, which is also Gaussian. Then, the absolute value is Rayleigh distributed (type of fading assumed for the system model), and the square of the absolute value follows an exponential distribution. Nonetheless, we verify the correctness of the previous statement through simulations for $\mathrm{M} = 2$ and $\mathrm{M} = 4$ as shown in Figure 10. Since both numerator and denominator are RVs, then, Z is also a RV. Finding

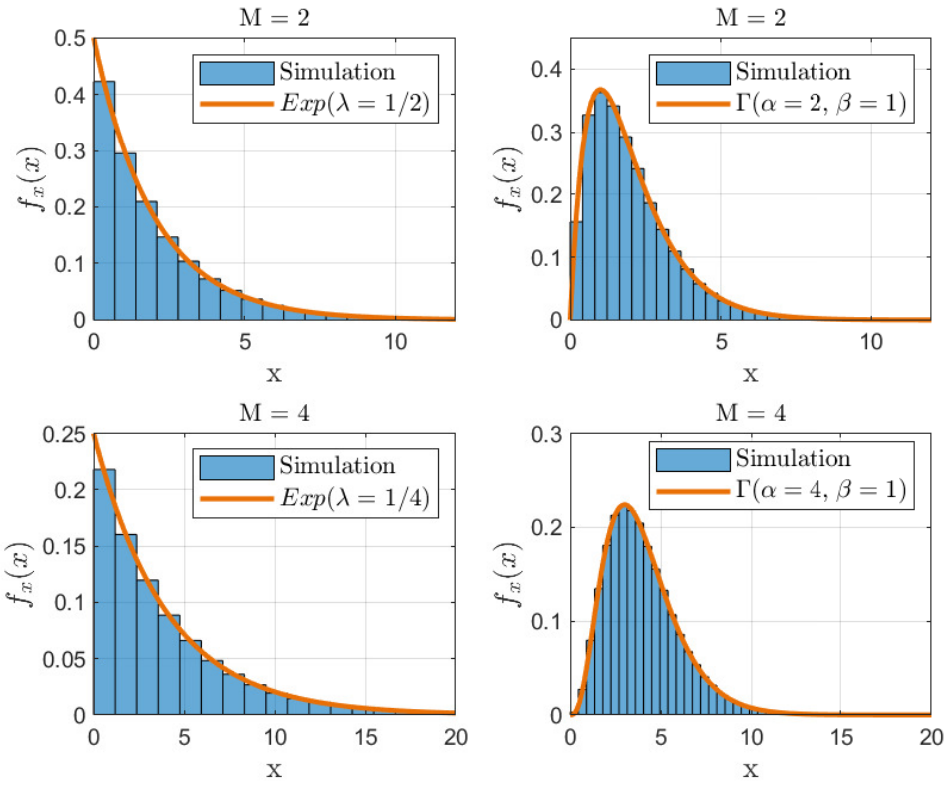

Figure 10. Fitting of numerator and denominator of Z to exponential and gamma distributions, respectively.

its distribution is crucial for further analysis but also a complicated task. The concept of radio distribution is applicable for uncorrelated RVs, however, Z is defined as the ratio of two correlated random variables since the same channel coefficients are present in both numerator and denominator. Instead of mathematical formulations, we resort to simulations to approximate the distribution of Z to a known distribution.

Lemma 1. *The RV Z approximately follows a Generalized Pareto Distribution (GPD) such that*

$$f_{\mathrm{Z}}(z) \approx \frac{\mathrm{M}-1}{\mathrm{M}}\left(1-\frac{z}{\mathrm{M}}\right)^{\mathrm{M}-2}. \tag{9}$$

Proof. Figure 11 shows the histograms and the approximations for different values of M. Surprisingly, results show that the histograms fit perfectly to the GPD. The approximation to the probability density function (PDF) is then

$$f_{\mu,\sigma,\xi}(z) \approx \frac{1}{\sigma}\left(1+\frac{\xi(z-\mu)}{\sigma}\right)^{\left(-\frac{1}{\xi}-1\right)}. \tag{10}$$

The parameters are: location μ, scale σ, and shape ξ. The corresponding values of these parameters are displayed in the plots. If we look carefully at the results, we can notice a clear relation of $\mu, \sigma,$ and ξ with M, which is, $\xi = -1/(\mathrm{M}-1)$, $\sigma = \mathrm{M}/(\mathrm{M}-1)$ and $\mu = 0$. Hence, we can substitute these values in (10) and rewrite the expression as a function of M, obtaining (9). □

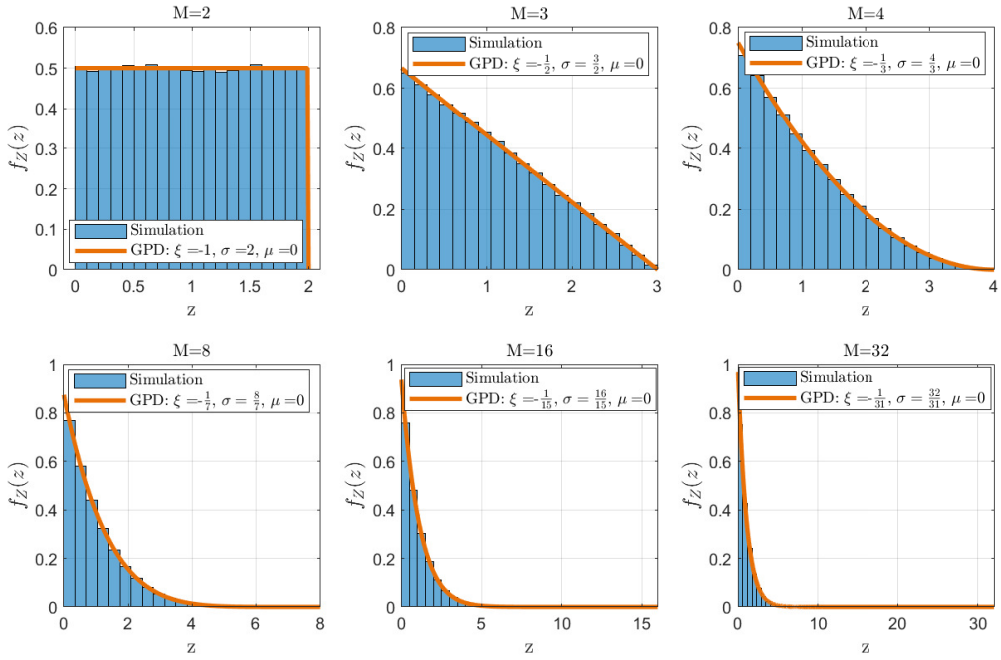

Figure 11. Fitting of the GPD to Z for M ∈ (2, 3, 4, 8, 16, 32).

It is worth pointing out that GPD approaches to an exponential RV when both μ and ξ are zero, which occurs when $\mathrm{M} \to \infty$ and its values range from 0 to M with expected value equals to 1 ($E[z] = \mu - \frac{\sigma}{1-\xi}$). Since the distribution of Z is now available, we can proceed to find the distribution of $\mathrm{P_{EH}}$

Theorem 1. *The distribution of* $\mathrm{P_{EH}}$ *is*

$$f_{\mathrm{P}_{EH}}(\mathrm{p}_{eh}) = \frac{(\mathrm{M}-1)\alpha_1}{\mathrm{M}(\alpha_1+\delta_1\mathrm{p}_{eh})^2}\left(1-\frac{\mathrm{p}_{eh}}{\mathrm{M}(\alpha_1+\delta_1\mathrm{p}_{eh})}\right)^{\mathrm{M}-2}, \tag{11}$$

where $\alpha_1 = \eta \mathrm{P}\varphi_g|g|^2\mathrm{P}_{RF}$ *and* $\delta_1 = \tau\eta\mathrm{P}\varphi_g|g|^2$.

Proof. We compute the distribution by applying the following transformation to RV Z

$$P_{\mathrm{EH}} = \frac{\alpha_1 Z}{1-\delta_1 Z}, \tag{12}$$

then, (11) follows immediately. □

3.2.3 Outage probability

With the PDF of the harvested power in place, we can proceed to derive the outage probabilities for both UL and DL. Lets first define the outage events at the *SBS* and *D* as $\mathbb{O}_{sbs} \triangleq \{(1-\tau)\log_2(1+\gamma_{\mathrm{sbs}}) < r_{sbs}\}$ and $\mathbb{O}_d \triangleq \{\tau\log_2(1+\gamma_{\mathrm{d}}) < r_d\}$, respectively.

Theorem 2. *The outage probability at the SBS in HD mode is given by*

$$\mathbb{P}\{\mathbb{O}_{sbs}\} = \frac{1}{\Gamma(\mathrm{M})}\Gamma\left(\mathrm{M}, \frac{(2^{\frac{r_{sbs}}{1-\tau}}-1)\sigma^2}{P_u\varphi_{ur}}\right). \tag{13}$$

Proof. The outage probability is computed as follows

$$\begin{aligned}\mathbb{P}\{\mathbb{O}_{sbs}\} &\overset{(a)}{=}\mathbb{P}\{(1-\tau)\log_2(1+\gamma_{\rm sbs})<r_{sbs}\}\\ &\overset{(b)}{=}\mathbb{P}\{(1-\tau)\log_2(1+\frac{\varphi_{\rm ur}{\rm P_u}||\mathbf{h}_{\rm ur}||^2}{\sigma^2})<r_{sbs}\}\\ &\overset{(c)}{=}\mathbb{P}\left\{||\mathbf{h}_{\rm ur}||^2<\frac{(2^{\frac{r_{sbs}}{1-\tau}}-1)\sigma^2}{{\rm P_u}\varphi_{\rm ur}}\right\}\\ &\overset{(d)}{=}\frac{1}{\Gamma({\rm M})}\Gamma\left({\rm M},\frac{(2^{\frac{r_{sbs}}{1-\tau}}-1)\sigma^2}{{\rm P_u}\varphi_{\rm ur}}\right),\end{aligned}$$

where (b) comes from substituting (4) in (a), (c) is the result of isolating $||\mathbf{h_{ur}}||^2$ in (b), and (d) comes from evaluating the cumulative density function (CDF) of a gamma RV on the right hand-side of the inequality in (c). □

Theorem 3. *The outage probability at D in HD mode is*

$$\mathbb{P}\{\mathbb{O}_d\}=1-\frac{({\rm M}-1)!}{{\rm e}^{\alpha_2}}\sum_{k=0}^{{\rm M}-1}\sum_{j=0}^{k}\frac{\alpha_2^{k-j}}{j!(k-j)!}(-\delta_2{\rm M})^j\Gamma(j+1){}_1F_1(1+j,j+{\rm M},\delta_2{\rm M}),\quad(14)$$

where $\alpha_2=\dfrac{(2^{2r_d}-1)\sigma^2}{\tau{\rm P_{RF}}\varphi_{\rm td}}$ *and* $\delta_2=\dfrac{(2^{2r_d}-1)\sigma^2{\rm P}\eta\varphi_g}{{\rm P_{RF}}\varphi_{\rm td}}$.

Proof. We first define the outage condition and then derive the expression for $\mathbb{P}\{\mathbb{O}_d\}$ as follows

$$\begin{aligned}\mathbb{P}\{\mathbb{O}_d\} &\overset{(a)}{=}\mathbb{P}\left\{\tau\log_2(1+\gamma_{\rm d})<r_d\right\}\\ &\overset{(b)}{=}\mathbb{P}\left\{\tau\log_2(1+\frac{\varphi_{\rm td}({\rm P_{EH}}+{\rm P_{RF}})||\mathbf{h}_{\rm td}||^2}{\sigma^2})<r_d\right\}\\ &\overset{(c)}{=}\mathbb{P}\left\{2^{\frac{2r_d}{\tau}}-1>\frac{\varphi_{\rm td}({\rm P_{EH}}+{\rm P_{RF}})||\mathbf{h}_{\rm td}||^2}{\sigma^2}\right\}\\ &\overset{(d)}{=}\mathbb{P}\left\{\frac{(2^{\frac{2r_d}{\tau}}-1)\sigma^2(1-\tau\eta{\rm P}\varphi_g|g|^2\left|\sum_{i=1}^{\rm M}{\rm w}_{{\rm td},i}\right|^2)}{{\rm P_{RF}}\varphi_{\rm td}}>||\mathbf{h}_{\rm td}||^2\right\}\\ &\overset{(e)}{=}\mathbb{P}\{\alpha_2-\delta_2 z>||\mathbf{h}_{\rm td}||^2\}\\ &\overset{(f)}{=}1-\int_0^{\rm M}\frac{1}{\Gamma({\rm M})}\Gamma({\rm M},\alpha_2-\delta_2 z)\frac{{\rm M}-1}{\rm M}\left(1-\frac{z}{\rm M}\right)^{{\rm M}-2}dz\\ &\overset{(g)}{=}1-\frac{({\rm M}-1)!}{\rm M}\sum_{k=0}^{{\rm M}-1}\frac{1}{k!}\int_0^{\rm M}\frac{(\alpha_2-\delta_2 z)^k}{{\rm e}^{\alpha_2-\delta_2 z}}\left(1-\frac{z}{\rm M}\right)^{{\rm M}-2}dz\\ &\overset{(h)}{=}1-\frac{({\rm M}-1)!}{\rm M}\sum_{k=0}^{{\rm M}-1}\sum_{j=0}^{k}\frac{1}{k!}\binom{k}{j}\frac{{\alpha_2}^{(k-j)}}{{\rm e}^{\alpha_2}}\int_0^{\rm M}{\rm e}^{\delta_2 z}(-\delta_2 z)^j\left(1-\frac{z}{\rm M}\right)^{{\rm M}-2}dz\\ &\overset{(i)}{=}1-\frac{({\rm M}-1)!}{{\rm e}^{\alpha_2}}\sum_{k=0}^{{\rm M}-1}\sum_{j=0}^{k}\frac{\alpha_2^{k-j}}{j!(k-j)!}(-\delta_2{\rm M})^j\Gamma(j+1){}_1F_1(1+j,j+{\rm M},\delta_2{\rm M}),\end{aligned}$$

where (b) comes from using (2), (c) eliminates the logarithm, (d) results from substituting (8) in (c) and isolating $||\mathbf{h}_{\text{td}}||^2$, and (e) from a simplification in the notation. In (f), we changed the expression to the integral form containing the CDF of a gamma RV evaluated in $\alpha_2 - \delta_2 z$ and the PDF of the GPD in (9). In (g), we took the terms dependent on M out of the integral and applied the property $\Gamma(n+1, v) = n!\mathrm{e}^{-v} e_n(v)$ [150, Eq. (8.352 2)] to the upper incomplete gamma function, with $e_n(v) = \sum_{k=0}^{n} \frac{v^k}{k!}$. Moreover, in (h), we applied the binomial expansion [150, Eq. (1.111)] to $(\alpha_2 - \delta_2 z)^k$. Finally, we obtained (14) by performing some algebraic manipulations and computing the integral. □

At this point, we have computed mathematical expressions for the outage probabilities at both links in HD mode. Notice that the outage at D depends on P since the larger the number of sER antennas, the larger the amount of harvested energy, modifying the total power used for transmission. At the SBS side, P does not influences the performance due to the lack of a SI channel as we will see in FD mode.

3.3 Full-duplex mode

In this second scheme, we consider the same SBS but operating in FD mode. The set of Q RF-chains in divided in M for transmission and N for reception (M + N = Q). Moreover, the SBS is equipped with a circuit for SIC and transmission, reception, sER and SIC occur uninterruptedly. We assume other conditions similar to the HD case unless specified otherwise. Figure 12 shows the setup, where we can notice the presence of two additional links if we compare with HD, one is the SI channel (denoted with SI) and the interference channel UD.

3.3.1 Signal model

In this scenario, the collected power from sER is also characterized by (8), the only difference is the value of τ, fixed to 1 in FD. Now can proceed to compute the SINR at the SBS, let's first write the received signal in the link UR before MRC as

$$\mathbf{y}_{\text{sbs}} = \sqrt{\varphi_{\text{ur}} \mathrm{P}_{\text{u}}} \mathbf{h}_{\text{ur}} s_u + \sqrt{\varphi_{\text{SI}} (\mathrm{P}_{\text{EH}} + \mathrm{P}_{\text{RF}}) \zeta} \mathbf{w}_{\text{td}}^H \mathbf{G}_{\text{SI}} s_s + \mathbf{n}_{\text{s}}, \tag{15}$$

where φ_{SI} denotes the path gain in the SI link, ζ represents the SIC coefficient and $\mathbf{G}_{\text{SI}}$ is a M × N matrix, which we model in the same way as $\mathbf{G}$ for convenience. This assumption brings mathematical tractability, however, it is not practical when considering the SI channel since the knowledge of the channel makes possible to achieve quasi-perfect SIC,

taking the residual SI to the noise floor. The remaining terms are defined as in HD. After MRC the SINR at the SBS is given by

$$\begin{aligned}\gamma_{\mathrm{sbs}} =& \frac{|\sqrt{\varphi_{\mathrm{ur}}\mathrm{P_u}}\mathbf{w}_{\mathrm{ur}}^H\mathbf{h}_{\mathrm{ur}}s_u|^2}{|\sqrt{\varphi_{\mathrm{SI}}(\mathrm{P_{EH}}+\mathrm{P_{RF}})\zeta}\mathbf{w}_{\mathrm{ur}}^H\mathbf{G}_{\mathrm{SI}}^H\mathbf{w}_{\mathrm{td}}s_s|^2 + E\{|\mathbf{w}_{\mathrm{ur}}^H\mathbf{n}_{\mathrm{s}}|\}^2} \\ =& \frac{\varphi_{\mathrm{ur}}\mathrm{P_u}||\mathbf{h}_{\mathrm{ur}}||^2}{\varphi_{\mathrm{SI}}(\mathrm{P_{EH}}+\mathrm{P_{RF}})\zeta|\mathbf{w}_{\mathrm{ur}}^H\mathbf{G}_{\mathrm{SI}}^H\mathbf{w}_{\mathrm{td}}|^2+\sigma^2}, \\ =& \frac{\varphi_{\mathrm{ur}}\mathrm{P_u}||\mathbf{h}_{\mathrm{ur}}||^2}{\varphi_{\mathrm{SI}}(\mathrm{P_{EH}}+\mathrm{P_{RF}})\zeta|g_s|^2\Big|\sum_{i=1}^{\mathrm{M}}\mathrm{w}_{\mathrm{td},i}\Big|^2\Big|\sum_{j=1}^{\mathrm{N}}\mathrm{w}_{\mathrm{ur},j}\Big|^2+\sigma^2},\end{aligned} \tag{16}$$

where g_s depicts the links of the channel matrix $\mathbf{G}_{\mathrm{SI}}$. Now, the signal level at D is represented as

$$\mathrm{y_d} = \sqrt{\varphi_{\mathrm{td}}(\mathrm{P_{EH}}+\mathrm{P_{RF}})}\mathbf{w}_{\mathrm{td}}^H\mathbf{h}_{\mathrm{td}}s_s + \sqrt{\varphi_{\mathrm{ud}}\mathrm{P_u}}h_{\mathrm{ud}}s_u + n_{\mathrm{d}}, \tag{17}$$

where φ_{ud} depicts the path gain in UD and h_{ud} is a zero-mean unit-variance Gaussian RV that represents the channel coefficient in the same link. Therefore, the SINR is given by

$$\gamma_{\mathrm{d}} = \frac{|\sqrt{\varphi_{\mathrm{td}}(\mathrm{P_{EH}}+\mathrm{P_{RF}})}\mathbf{w}_{\mathrm{td}}^H\mathbf{h}_{\mathrm{td}}s_s|^2}{|\sqrt{\varphi_{\mathrm{ud}}\mathrm{P_u}}h_{\mathrm{ud}}s_u|^2+\sigma^2} = \frac{\varphi_{\mathrm{td}}(\mathrm{P_{EH}}+\mathrm{P_{RF}})||\mathbf{h}_{\mathrm{td}}||^2}{\varphi_{\mathrm{ud}}\mathrm{P_u}|h_{\mathrm{ud}}|^2+\sigma^2}. \tag{18}$$

3.3.2 Outage probability

With the expressions for the SINRs at the SBS and D we can derive the outage probabilities for both of them.

Theorem 4. *The outage probability at the SBS in FD mode given by*

$$\begin{aligned}\mathbb{P}\{\mathbb{O}_{sbs}\} =& 1-\beta(\mathrm{M}-1,\mathrm{N}-1)\sum_{i=0}^{\mathrm{N}-1}\sum_{l=0}^{i}\sum_{p=0}^{\mathrm{M}+\mathrm{N}-3}\frac{\delta_3^l\alpha_3^{i-l}(\mathrm{M}-1)(\mathrm{N}-1)}{i!\mathrm{e}^{\delta_3}}(-1)^p \\ &\times\binom{\mathrm{M}+\mathrm{N}-3}{\mathrm{p}}\binom{i}{l}(\mathrm{MN})^{i-l}\left(\sum_{s=1}^{n}w_s\Big[\mathrm{e}^u f(u)\Big]+\mathrm{R}_n(u)\right),\end{aligned} \tag{19}$$

where $\alpha_3 = \dfrac{(2^{r_d}-1)\zeta|g_s|^2\Big|\mathrm{P_{RF}}\varphi_{\mathrm{SI}}}{\mathrm{P_u}\varphi_{\mathrm{ur}}(1-\eta\mathrm{P}\varphi_g|g|^2)}$, $\delta_3 = \dfrac{\sigma^2}{\mathrm{P_u}\varphi_{\mathrm{ur}}}, u = -1+\dfrac{\mathrm{MN}}{q}$ *with* $q = \Big|\sum_{i=1}^{\mathrm{N}}\mathrm{w}_{\mathrm{ur},i}\Big|^2\Big|\sum_{j=1}^{\mathrm{M}}\mathrm{w}_{\mathrm{td},j}\Big|^2$.

Moreover,

$$\begin{aligned}w_s &= \frac{(n!)u_s}{(n+1)^2\Big[L_{n+1}(u_s)\Big]^2},\ R_n(u) = \frac{(n!)^2}{(2n)!}f^{(2n)}(u), \\ f(u) &= \mathrm{e}^{-\frac{\alpha_3\mathrm{MN}}{1+u}}(1+u)^{-3-i+l+\mathrm{N}-p}{}_2F_1(\mathrm{N}-1,\mathrm{N}-1,\mathrm{M}+\mathrm{N}-2,-u),\end{aligned}$$

with $L_n(u_k)$ *as the Laguerre polynomials and* u_s *their s-th root.*

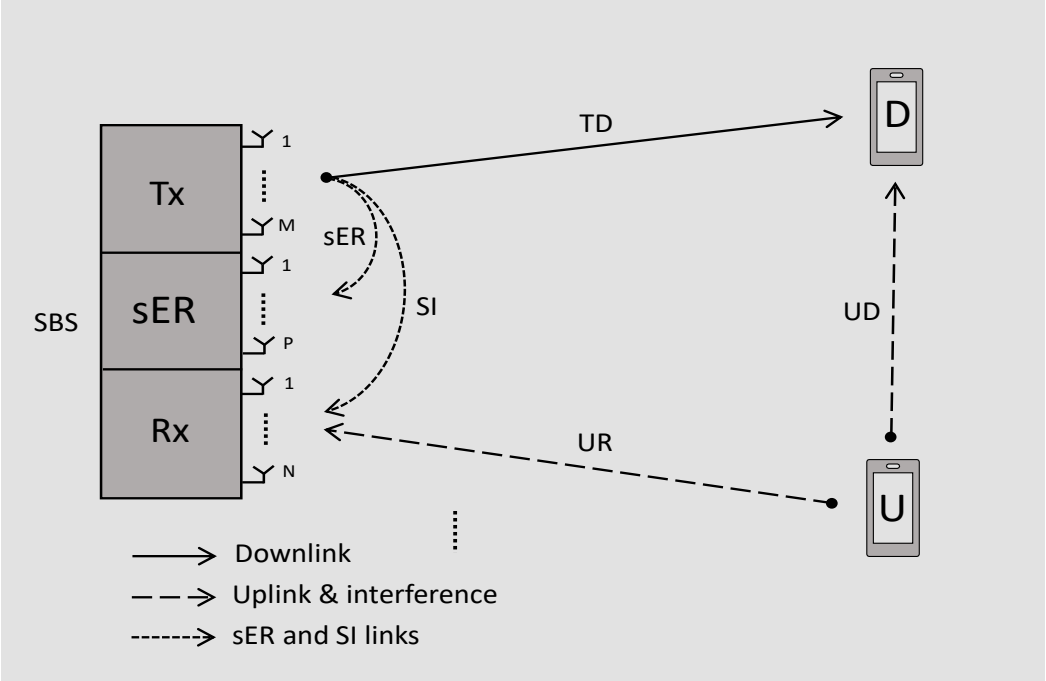

Figure 12. FD scheme. The SBS communicates with U and D via UL and DL channels, respectively. SI link at the SBS and interference between UL and DL are also included in this scheme.

Proof. Before deriving the expression for the outage, it is worth looking at the variable q, notice that it represents the product of two variables with same distribution since $\left|\sum_{i=1}^{\mathrm{N}} \mathrm{w}_{\mathrm{ur},i}\right|^2$ and $\left|\sum_{j=1}^{\mathrm{M}} \mathrm{w}_{\mathrm{td},j}\right|^2$ only differ in the number of elements in the summations. Hence, this represents the product of two GPD, whose distribution is required for finding the outage probability. The distribution of this product is presented in [151, Theorem 1] as

$$f_q(q) = \frac{1}{k_1 m_1}\left(\frac{c_1}{k_1}\right)^{\frac{1}{c_1}-1}\left(\frac{qd_1}{m_1}\right)^{-\frac{1}{d_1}}\left(\frac{k_1}{c_1}-\frac{qd_1}{m_1}\right)^{\frac{1}{c_1}+\frac{1}{d_1}-1}\beta\left(\frac{1}{c_1},\frac{1}{d_1}\right){}_2F_1\left(\frac{1}{d_1},\frac{1}{d_1},\frac{1}{c_1},1-\frac{k_1 m_1}{qd_1c_1}\right), \quad (20)$$

where $k_1 = \frac{\mathrm{M}}{\mathrm{M}-1}$, $m_1 = \frac{\mathrm{N}}{\mathrm{N}-1}$, $c_1 = \frac{1}{\mathrm{M}-1}$ and $d_1 = \frac{1}{\mathrm{N}-1}$ for our specific setup. We checked the accuracy of the expression for different values of M and N. We can notice in Figure 13 that the simulations match with the analytical expressions. Lets now derive the expression for the outage probability as follows

$$\begin{aligned}
\mathbb{P}\{\mathbb{O}_{sbs}\} &\overset{(a)}{=} \mathbb{P}\{\log_2(1+\gamma_{\mathrm{sbs}}) < r_{sbs}\} \\
&\overset{(b)}{=} \mathbb{P}\{\log_2(1+\frac{\varphi_{\mathrm{ur}}\mathrm{P_u}||\mathbf{h}_{\mathrm{ur}}||^2}{\varphi_{\mathrm{SI}}(\mathrm{P_{EH}}+\mathrm{P_{RF}})\zeta|^2 g_s\left|\sum_{i=1}^{\mathrm{M}}\mathrm{w}_{\mathrm{td},i}\right|^2\left|\sum_{j=1}^{\mathrm{N}}\mathrm{w}_{\mathrm{ur},j}\right|^2+\sigma^2}) < r_{sbs}\} \\
&\overset{(c)}{=} \mathbb{P}\{||\mathbf{h}_{\mathrm{ur}}||^2 < \alpha_3 q + \delta_3\},
\end{aligned}$$

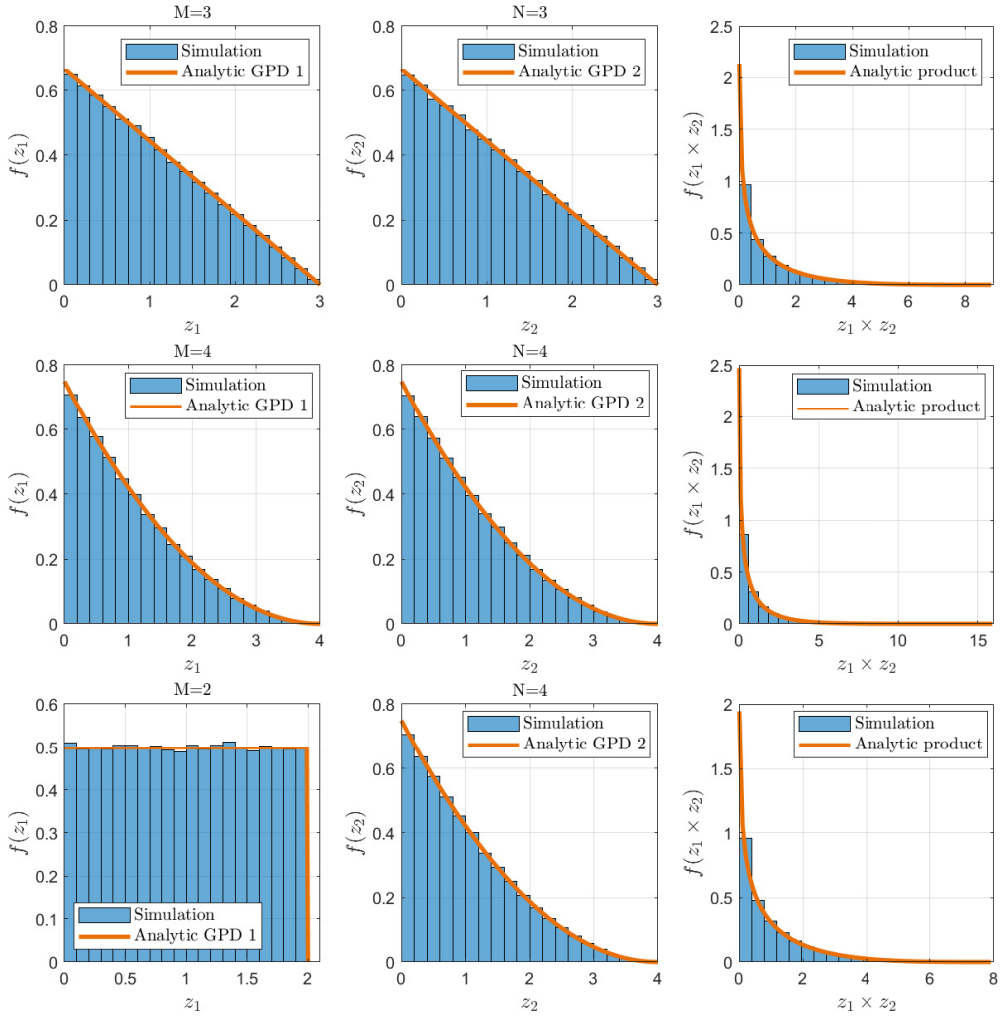

Figure 13. Simulation and analytical expression of the product of two GPDs, z_1 and z_2 represent RV 1 and RV 2, respectively.

$$\overset{\text{(d)}}{=} 1-\frac{1}{\Gamma(\mathrm{N})}\int_0^{\mathrm{MN}}\Gamma(\mathrm{N},\alpha_3 q+\delta_3)\frac{1}{k_1 m_1}\left(\frac{c_1}{k_1}\right)^{\frac{1}{c_1}-1}\left(\frac{qd_1}{m_1}\right)^{-\frac{1}{d_1}}\left(\frac{k_1}{c_1}-\frac{qd_1}{m_1}\right)^{\frac{1}{c_1}+\frac{1}{d_1}-1}$$
$$\times\beta\left(\frac{1}{c_1},\frac{1}{d_1}\right){}_2F_1\left(\frac{1}{d_1},\frac{1}{d_1},\frac{1}{c_1},1-\frac{k_1 m_1}{qd_1 c_1}\right)dq$$

$$\overset{\text{(e)}}{=} 1-\frac{1}{\Gamma(\mathrm{N})}\int_0^{\mathrm{MN}}\Gamma(\mathrm{N},\alpha_3 q+\delta_3)(\mathrm{M}-1)(\mathrm{N}-1)\left(\frac{1}{\mathrm{M}}\right)^{\mathrm{M}-1}\left(\frac{q}{\mathrm{N}}\right)^{-\mathrm{N}+2}\left(\mathrm{M}-\frac{q}{\mathrm{N}}\right)^{\mathrm{M}+\mathrm{N}-3}$$
$$\times\,\beta(\mathrm{M}-1,\mathrm{N}-1){}_2F_1\left(\mathrm{N}-1,\mathrm{N}-1,\mathrm{M}+\mathrm{N}-2,1-\frac{\mathrm{MN}}{q}\right)dq$$

$$\overset{\text{(f)}}{=} 1-\beta(\mathrm{M}-1,\mathrm{N}-1)\sum_{i=0}^{\mathrm{N}-1}\sum_{l=0}^{i}\sum_{p=0}^{\mathrm{M}+\mathrm{N}-3}\frac{\delta_3^l\alpha_3^{i-l}(\mathrm{M}-1)(\mathrm{N}-1)}{i!\mathrm{e}^{\delta_3}}(-1)^p\binom{\mathrm{M}+\mathrm{N}-3}{p}\binom{i}{l}$$
$$\times\left(\frac{1}{\mathrm{MN}}\right)^{-\mathrm{N}+p+2}\int_0^{\mathrm{MN}}\mathrm{e}^{-\alpha_3 q}q^{i-l-\mathrm{N}+p+1}{}_2F_1\left(\mathrm{N}-1,\mathrm{N}-1,\mathrm{M}+\mathrm{N}-2,1-\frac{\mathrm{MN}}{q}\right)dq$$

$$\overset{\text{(g)}}{=} 1-\beta(\mathrm{M}-1,\mathrm{N}-1)\sum_{i=0}^{\mathrm{N}-1}\sum_{l=0}^{i}\sum_{p=0}^{\mathrm{M}+\mathrm{N}-3}\frac{\delta_3^l\alpha_3^{i-l}(\mathrm{M}-1)(\mathrm{N}-1)}{i!\mathrm{e}^{\delta_3}}(-1)^p\binom{\mathrm{M}+\mathrm{N}-3}{p}\binom{i}{l}$$
$$\times(\mathrm{MN})^{i-l}\int_0^{\infty}\mathrm{e}^{-\frac{\alpha_3\mathrm{MN}}{1+u}}(1+u)^{-3-i+l+\mathrm{N}-p}{}_2F_1(\mathrm{N}-1,\mathrm{N}-1,\mathrm{M}+\mathrm{N},-u)du$$

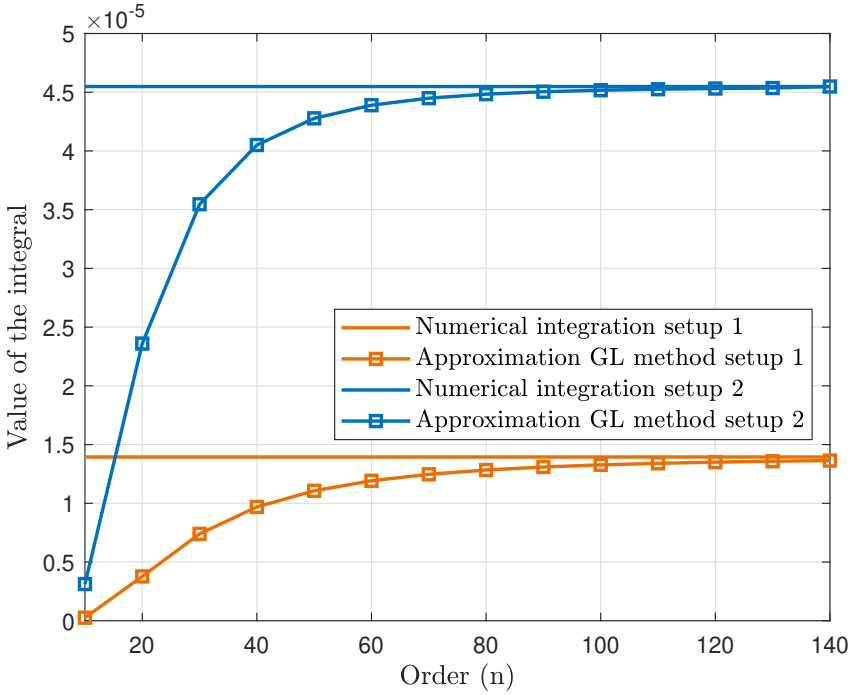

Figure 14. Accuracy and convergence of the GL method for two setups.

$$\overset{(h)}{=} 1-\beta(\mathrm{M}-1,\mathrm{N}-1)\sum_{i=0}^{\mathrm{N}-1}\sum_{l=0}^{i}\sum_{p=0}^{\mathrm{M+N-3}}\frac{\delta_3^l\alpha_3^{i-l}(\mathrm{M}-1)(\mathrm{N}-1)}{i!\mathrm{e}^{\delta_3}}(-1)^p\binom{\mathrm{M+N}-3}{p}\binom{i}{l}$$
$$\times(\mathrm{MN})^{i-l}\left(\sum_{s=1}^{n}w_s\left[\mathrm{e}^u f(u)\right]+R_n(u)\right),$$

where (b) comes from substituting (16) in (a), (c) results from isolating $||h_{ur}||^2$ and simplifying the notation, (d) represents the integral of the CDF of a gamma RV weighted by the PDF in (20), in (e) we put the expression as a function of M and N, and (f) comes from using [150, Eq. (1.111)] and from applying the binomial expansion to the term $\left(\mathrm{M}-\frac{q}{\mathrm{N}}\right)^{\mathrm{M+N-3}}$. The integral in (f) is difficult to solve, hence, we changed the integration limits and the variable to u in (g), as stated in Theorem 4. Now, the integral is in the form $\int_0^\infty \mathrm{e}^{-\mathrm{u}}\left[\mathrm{e}^{\mathrm{u}}f(u)\right]du$ and can be efficiently solved using the Gauss-Laguerre (GL) method [152, Eq.(25.4.45)] as in (h). The GL formula is defined as follows

$$\int_0^\infty \mathrm{e}^{-x}\left[\mathrm{e}^x f(x)dx\right]=\sum_{s=1}^{n}w_s\left[\mathrm{e}^x f(x)\right]+R_n(x), \tag{21}$$

where w_s and $R_n(x)$ are defined in the theorem. In this method, the computation of the residual is dependent on the existence of high-order derivatives of $f(x)$. We show in Figure 14 the convergence of the GL method when computing the integral. The figure displays the numerical value of the integral and the method for two setups. Notice that for orders higher than 60 the method approaches the real values of the integral. Table 3 shows the values used for the simulations.

□

Table 2. Values for checking the accuracy of GL method.

Setup	M	N	α_3	l	p	i
1	3	4	20	2	2	2
2	2	2	46	4	4	2

Theorem 5. *The outage probability at D in FD mode is given by*

$$\mathbb{P}\{\mathbb{O}_d\} = 1 - \mathrm{e}^{\alpha_4}(1 - (1+\delta_4)^{-\mathrm{M}}), \tag{22}$$

where $\alpha_4 = \dfrac{\sigma^2}{\varphi_{ud}\mathrm{P_u}}$ *and* $\delta_4 = \dfrac{\varphi_{td}\mathrm{P_{RF}}}{\varphi_{ud}\mathrm{P_u}(2^{r_d}-1)(1-\eta\mathrm{P}\varphi_g|g|^2)}$.

Proof. We proceed as follows

$$\begin{aligned}
\mathbb{P}\{\mathbb{O}_d\} &\overset{(a)}{=} \mathbb{P}\{\log_2(1+\gamma_{\mathrm{d}}) < r_d\} \\
&\overset{(b)}{=} \mathbb{P}\left\{2^{r_d}-1 > \frac{\varphi_{\mathrm{td}}\mathrm{P_{RF}}||\mathbf{h}_{\mathrm{td}}||^2}{(\varphi_{\mathrm{ud}}\mathrm{P_u}|h_{\mathrm{ud}}|^2+\sigma^2)(1-\tau\eta\mathrm{P}\varphi_g|g|^2\left|\sum_{i=1}^{\mathrm{M}}\mathrm{w}_{\mathrm{td},i}\right|^2)}\right\} \\
&\overset{(c)}{=} \mathbb{P}\left\{\frac{|h_{\mathrm{ud}}|^2+\frac{\sigma^2}{\varphi_{\mathrm{ud}}\mathrm{P_u}}}{||\mathbf{h}_{\mathrm{td}}||^2} > \frac{\varphi_{\mathrm{td}}\mathrm{P_{RF}}}{\varphi_{\mathrm{ud}}\mathrm{P_u}(2^{r_d}-1)(1-\tau\eta\mathrm{P}\varphi_g|g|^2\left|\sum_{i=1}^{\mathrm{M}}\mathrm{w}_{\mathrm{td},i}\right|^2)}\right\} \\
&\overset{(d)}{\approx} 1 - \frac{1}{\Gamma(\mathrm{M})}\int_0^{b_3}\int_0^{\infty}\mathrm{e}^{(a_3-\mathrm{ry})}\mathrm{e}^{-\mathrm{y}}\mathrm{y}^{\mathrm{M}}d\mathrm{y}d\mathrm{r} \\
&\overset{(e)}{=} 1 - \mathrm{e}^{\alpha_4}(1-(1+\delta_4)^{-\mathrm{M}}),
\end{aligned}$$

where (b) is obtained by substituting (8) and (18) into (a), (c) comes after some manipulations to get the ratio of a shifted exponential and a gamma random variable, (d) is an approximation since we ignored the term $\left|\sum_{i=1}^{\mathrm{M}}\mathrm{w}_{\mathrm{td},i}\right|^2$ in the denominator because $\tau\eta\mathrm{P}\varphi_g|g|^2$ is small. Then, the concept of ratio distribution is applied, e.g. $\mathrm{p_R(r)} = \int_0^{\infty}\mathrm{y}\mathrm{p_{X,Y}(ry,y)dy}$ with $\mathrm{R = X/Y}$. Finally, we obtained the result in (e) after computing both integrals. □

3.3.3 Optimal antenna allocation

Herein, we assume the FD SBS switches the antennas between transmission and reception as required, which is possible considering state-of-the-art transceivers [153]. As mentioned before, the outage probability is a good metric for measuring reliability, hence, in order to achieve maximum fairness between both links we minimize the maximum (MinMax) outage probability in the network by dynamically determining the optimum number of transmit and receive antennas from the total. This approach is also applicable to networks with multiple UL and DL devices. It is worth mentioning that the network information is not required at U nor at D since they are single antenna devices and cannot perform any multiantenna technique. Hence, the dynamic FD scheme is stated as

$$\mathbf{P1}: \quad \min_{\mathrm{M,N}} \quad \max_{i\in\{D,SBS\}} \ \mathbb{P}\{\mathbb{O}_i\} \tag{23a}$$

$$\text{s.t.} \quad \mathrm{M}+\mathrm{N}=\mathrm{Q} \tag{23b}$$

$$\mathrm{M},\mathrm{N}\geq 2 \tag{23c}$$

Moreover, we can set a MinMax reliability target and determine the minimum amount of RF chains required to achieve it. This is because we can think of an SBS that has a large number of RF chains but might not be necessary to used all of them, instead, the minimum amount which guarantees the required reliability is activated while the others remain idle.

$$\mathbf{P2}: \quad \min_{\mathrm{M,N}} \quad \mathrm{Q} \tag{24a}$$

$$\text{s.t.} \quad \mathrm{M}+\mathrm{N}=\mathrm{Q} \tag{24b}$$

$$\mathrm{M},\mathrm{N}\geq 2 \tag{24c}$$

$$\mathbb{P}\{\mathbb{O}_i\}\leq\chi \tag{24d}$$

where χ is the target value. In typical scenarios small values of M, N and Q are practical, then, we can find the solution to P_1 and P_2 using a "brute-force search" instead of resorting to more complex methods. Numerical solutions to these problems are presented and discussed in Chapter 4.

3.4 Power consumption model

Herein, we discuss a practical model for the energy consumption in the RF chains. We adopt the model proposed in [154], which defines the total power consumption as the sum of the consumption of the power amplifiers (PA) $\mathrm{P_{pow}}$, and other circuit blocks $\mathrm{P_c}$. $\mathrm{P_{pow}}$ is computed as

$$\mathrm{P_{pow}}=(1+\theta)\mathrm{P_{RF}}, \tag{25}$$

where $\theta=(\epsilon/\eta_{pow})-1$ with $\eta_{pow}\in(0,1)$ as the drain efficiency of the PAs and ϵ is the peak-to-average ratio. The consumption of other blocks is given by

$$\mathrm{P_c}=\mathrm{M}(\mathrm{P_{dac}}+\mathrm{P_{mix}}+\mathrm{P_{filt}})+2\mathrm{P_{syn}}+\mathrm{N}(\mathrm{P_{lna}}+\mathrm{P_{mix}}+\mathrm{P_{ifa}}+\mathrm{P_{filr}}+\mathrm{P_{adc}}), \tag{26}$$

where $\mathrm{P_{dac}},\mathrm{P_{mix}},\mathrm{P_{lna}},\mathrm{P_{ifa}},\mathrm{P_{filt}},\mathrm{P_{filr}},\mathrm{P_{adc}}$ and $\mathrm{P_{syn}}$ depict the consumption of digital to analog converters (DAC), mixers, the low-noise amplifiers, intermediate frequency amplifiers, active filters at the transmitter side, active filters at the receiver side, ADCs and frequency synthesizers, respectively. Hence, the transmit power is defined as

$$\mathrm{P_{RF}}=\frac{\mathrm{P_G}-\mathrm{P_c}}{1-\theta}. \tag{27}$$

4 NUMERICAL RESULTS

In this chapter we check the accuracy of the expressions for the outage probabilities through Monte Carlo simulations. Moreover, we present numerical solutions to optimization problems **P1** and **P2** and analyze the impact of network parameters on the system performance.

4.1 Accuracy of outage probability expressions

The first step is to check the accuracy of the obtained analytical expressions for outage probabilities in both HD and FD scenarios. We analyze two cases: i) ideal, where the power consumed by the hardware is not considered, i.e., $\mathrm{P_{RF}} = \mathrm{P_G}$, and ii) practical, where the hardware power consumption is taken into account, i.e., $\mathrm{P_{RF}} = (\mathrm{P}_G - \mathrm{P_c})/(1-\alpha)$ as discussed in Section 3.4. Table 3 shows the value of the system parameters utilized for the simulations, these values remain equal unless stated otherwise.

The values of the power consumption of active elements were taken from [154]. The transmission rates are typical in multi-antenna systems where even higher values are possible in the high SNR regime. We assumed a symmetric HD scheme, i.e., $\tau = 0.5$, and the rest of the parameters are also practical. In the particular case of SIC, we assumed a high enough value, relying on the assumption that an efficient technique is used. Figure 15 shows the behaviour of the outage probability in the DL for different values of ζ. From now one we assume $\zeta = 100$ dB since the performance for this value is not considerably degraded according to results in Figure 15, and it is attainable in practice [66, 155]. Moreover, U and D are assumed to be far enough such that we can ignore the effect of the interference at D, allowing a fairer comparison between HD and FD schemes.

Table 3. Simulation parameters.

Parameter	**Value**	
Q	16	
$\mathrm{P_{dac}}, \mathrm{P_{adc}}$	1 mW	[154]
$\mathrm{P_{mix}}$	30.3 mW	[154]
$\mathrm{P_{lna}}$	20 mW	[154]
$\mathrm{P_{ifa}}$	3 mW	[154]
$\mathrm{P_{filt}}, \mathrm{P_{filr}}$	2.5 mW	[154]
$\mathrm{P_{syn}}$	50 mW	[154]
σ^2	0.1 nW	
η	0.5	
$\mathrm{P_G}$	15 W	
P	{0, 8}	
$\mathrm{P_u}$	100 mW	
ζ	-100 dB	[66, 155]
φ_g	-15 dB	[118]
φ_{ud}	-60 dB	

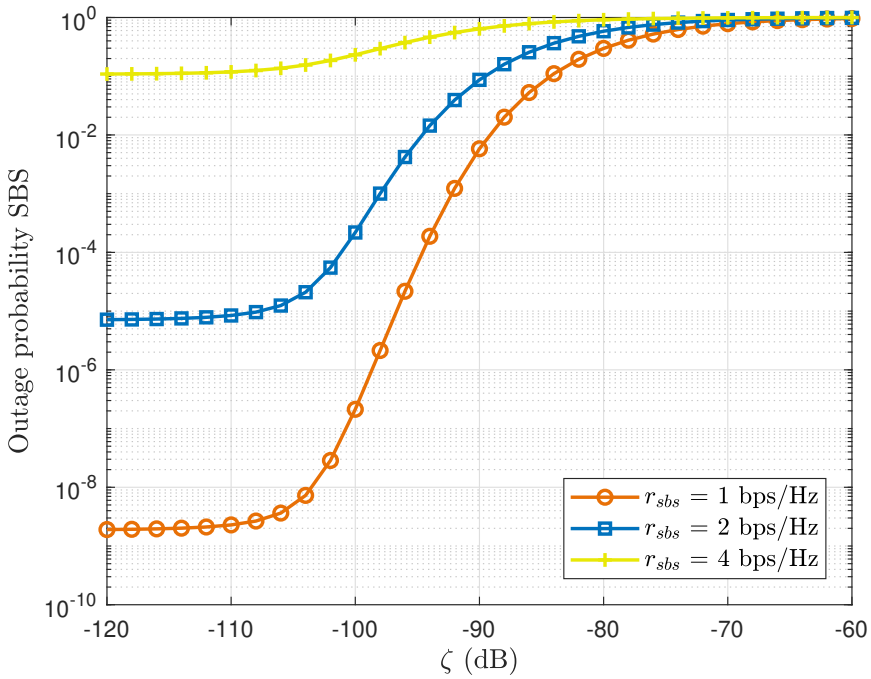

Figure 15. Outage probability at the SBS vs SIC.

Figure 16 shows the outage performance for HD and FD scenarios. In Figure 16 (a), it can be noticed a considerable performance gap in the link TD between the practical and the ideal HD case. Notice that when the circuit power consumption in the RF chains is considered, there is less power available for transmission; however, this consumption does not harm the outage probability at the SBS at all. Figure 16 (b) shows the same comparison at D but for the FD scenario. Similarly, the performance is worse when considering the practical case since the signal is transmitted with less power. On the other hand, and differently from the HD scenario, the performance at the SBS is better when comparing to the ideal case. This is because the lower the transmission power, the lower the self-interference level, which translates to an improvement in terms of outage probability.

4.2 Performance of the dynamic FD scheme

Figure 17 shows the maximum outage probability between UL and DL as a function of the number of transmit antennas and for different values of r_d. Obviously, there is an optimum operational point which guarantees the best minimum level of reliability among the devices in the network. It can be noticed how the optimal combination of transmit (x-axis) and receive antennas is the one with the closest points between both curves. This is because we are distributing the antennas between transmission and reception, thus, we cannot decrease the outage events at both devices simultaneously. Then, a larger number of antennas for transmission will decrease the outage probability at D but will increase it at the SBS. It is worth noting the effect of sER in the performance. We can see in Figure 17 (a) how the optimal number of transmit antennas are 4, 4, 6 and 8 for the 4 different

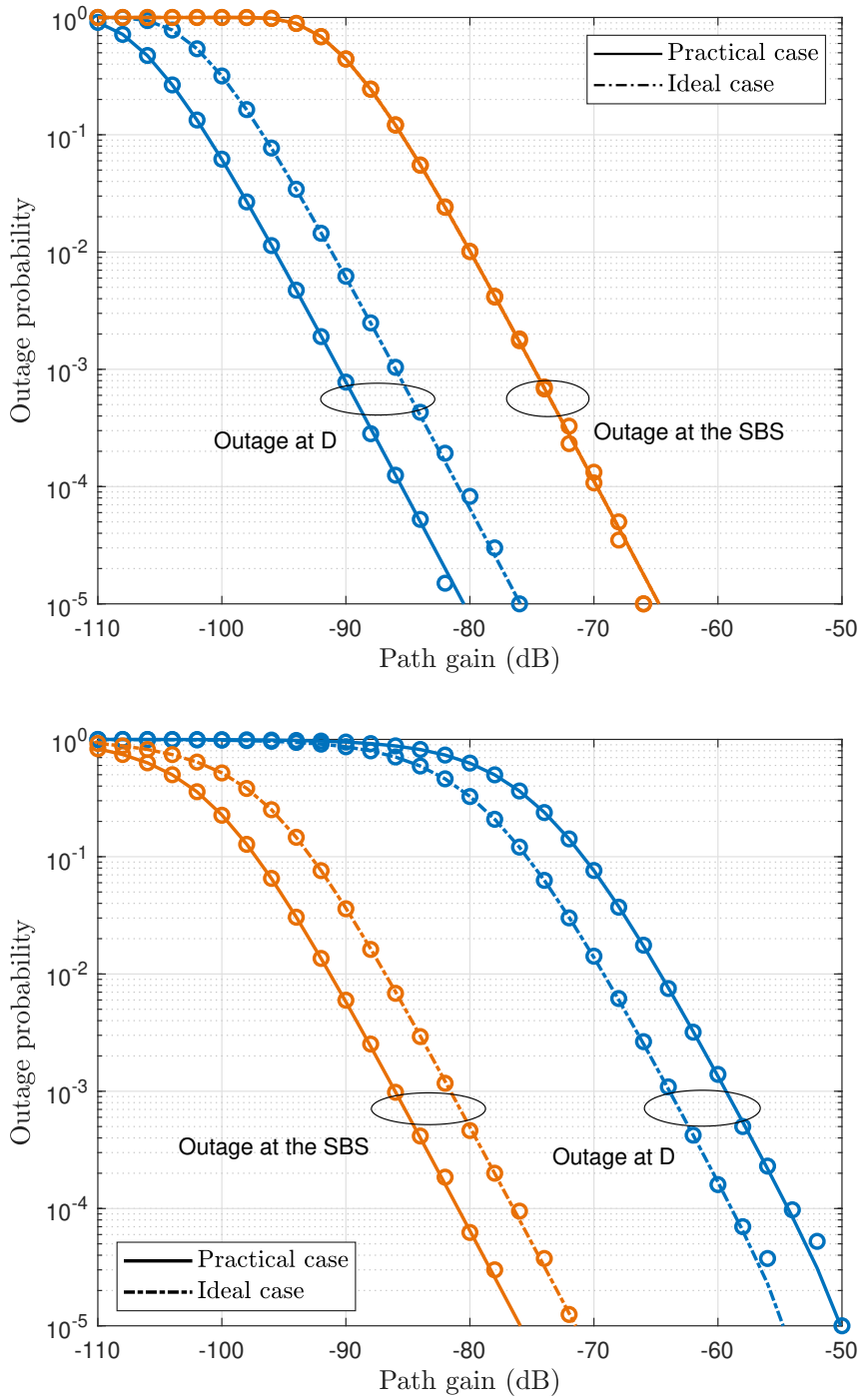

Figure 16. Outage probability as function of φ_{td} and φ_{ur}. (a) HD (top). (b) FD (bottom). φ_{ud} = -60 dB. Markers represent Monte Carlo simulations.

r_d values without sER, while 3, 4, 5 and 8 are the optimal ones when 8 antennas are used as shown in Figure 17 (b). This is because with recycling antennas, the available power is $\text{P}_{\text{RF}} + \text{P}_{\text{EH}}$, which causes a variation in the probabilities and therefore different optimal combinations. The number of transmit and receive antennas will also depend on the service requirements. For instance, it can be seen that if the requirements are close

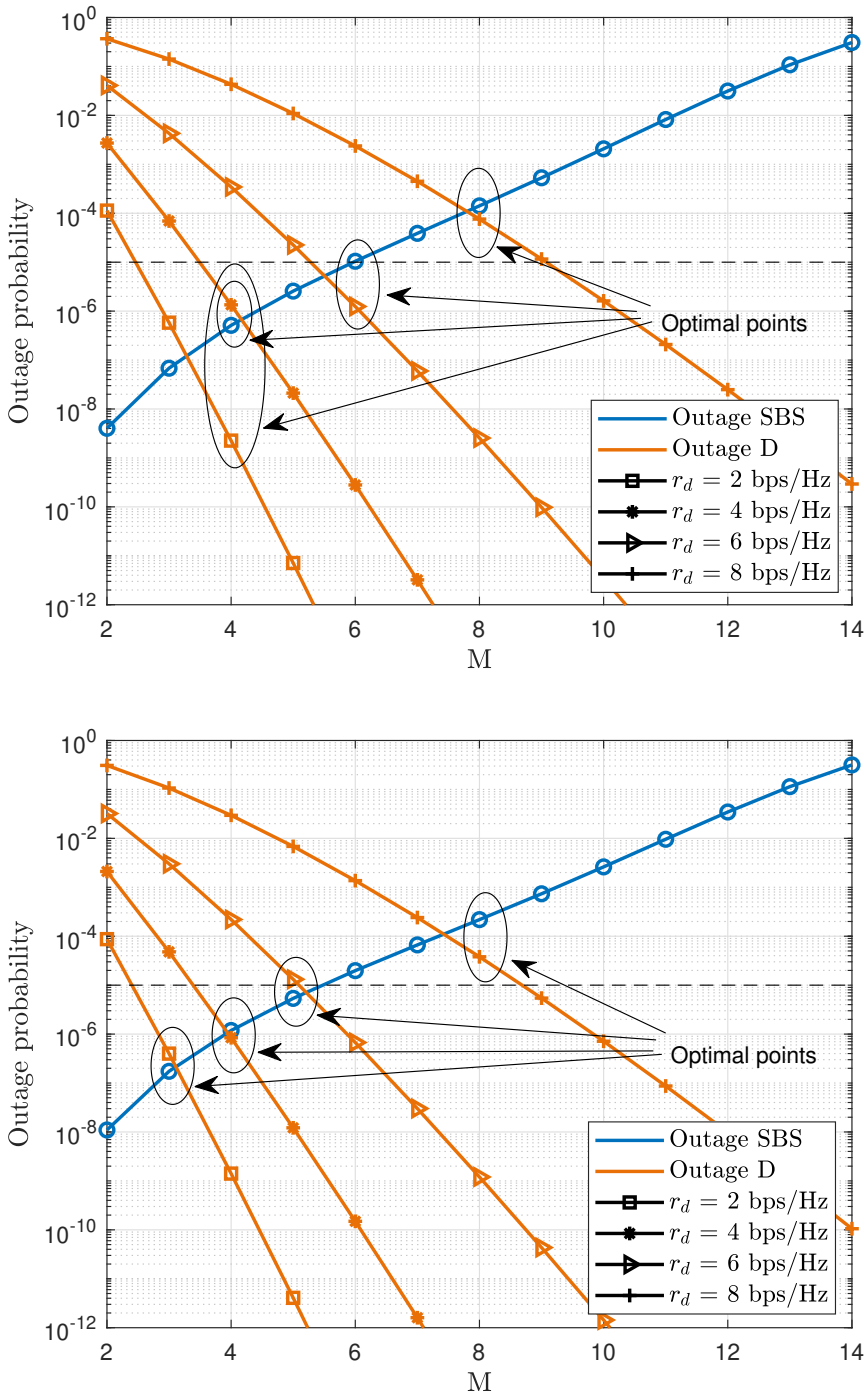

Figure 17. Optimal points FD. (a) No EH (top). (b) 8 EH antennas (bottom). $r_{sbs} = 2$ bps/Hz and $\varphi_{\text{ur}} = \varphi_{\text{td}} = -85$ dB. The area below the dashed lines represents the URC region.

to 10^{-5} with $r_d = 6$ bps/Hz, the combination that achieves the best performance is 5 transmit and 11 receive antennas. On the other hand, if the required outage probability changes to 10^{-3} under the same network configuration, then, in addition to the optimal combination, 4 to 9 transmit antennas can be used since both D and the SBS will fulfill

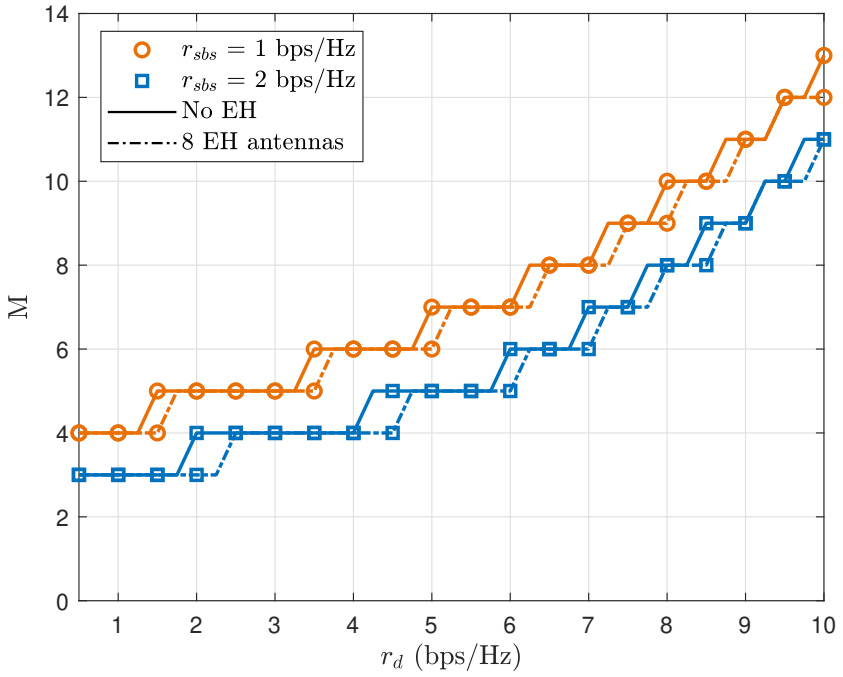

Figure 18. Optimal number of Tx antennas vs r_d. $\varphi_{\text{ur}} = \varphi_{\text{td}}$ = -85 dB and $Q = 16$.

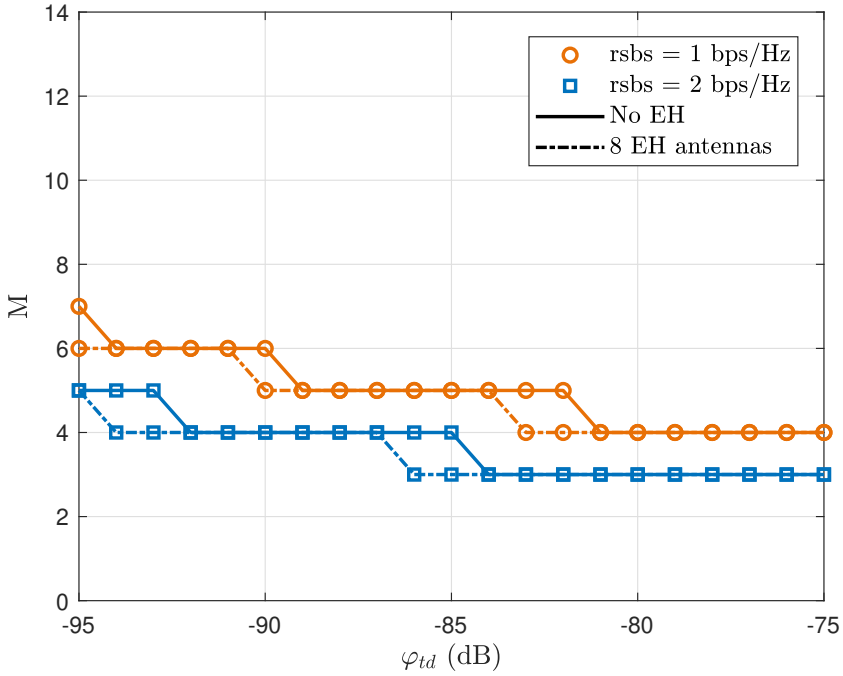

Figure 19. Optimal number of Tx antennas vs path gain. $r_d = 2$ bps/Hz, $\varphi_{\text{ur}} = -85$ dB and $Q = 16$.

the requirements. Finding the optimal number of Tx and Rx antennas brings fairness between both links, this is because they can operate with a performance as close as possible to each other. In Figure 17 (a), for $r_d = 6$ bps/Hz, we can notice that if we fix

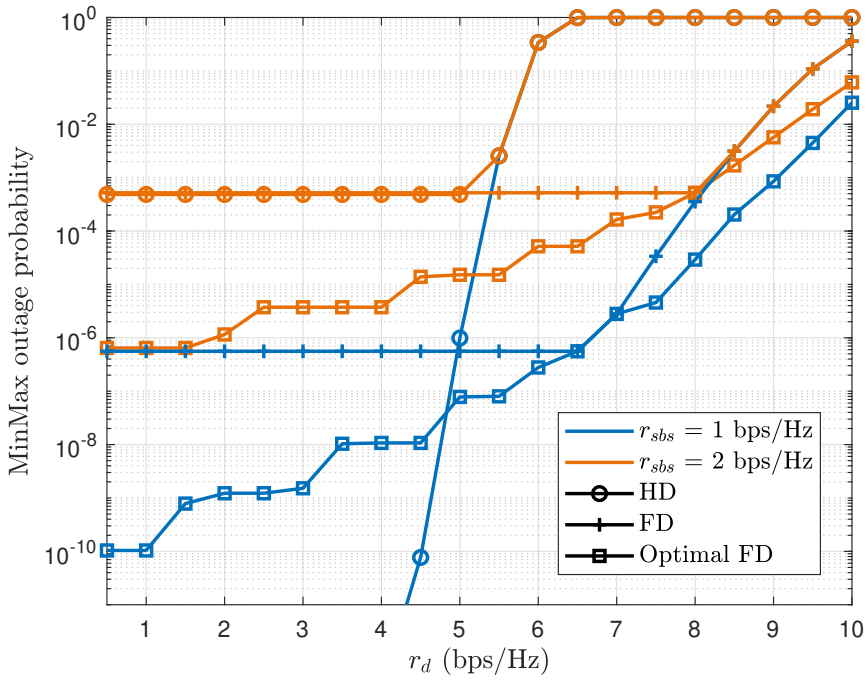

Figure 20. MinMax outage probability. Dynamic FD, FD and HD.

M = N = 8, the outage probabilities are in the order of 10^{-4} at the SBS and 10^{-8} at D, however, using the optimal configuration of M = 6 and N = 10 both links operate in the URC region simultaneously, i.e., achieving outage probabilities around 10^{-5} and 10^{-6} at D and the SBS, respectively.

Figures 18 and 19 show the optimal number of transmit antennas as a function of r_d and path gain, respectively. In Figure 18 we can notice that the larger the value of r_d, the larger the number of transmit antennas required for achieving the optimal performance. On the other hand, Figure 19 shows how for larger values of path gain (path gain = path loss^{-1}), the number of antennas required for transmission decreases since the SNR at D is higher, thus, the outage probability decreases. This fact allows the SBS to use one of the transmit antennas in reception for improving the outage probability in UR since in the TD link there is a gain in terms of SNR.

Figure 20 compares the performance of a dynamic FD scheme, under which the SBS determines the optimal configuration dynamically based on the network parameters by solving **P1**, a simple FD with half of the antennas for transmission and half for reception, and an HD scheme using all 16 antennas for both transmission and reception. It shows the performance as a function of r_d and r_{sbs}, while we set the path gain to -85 dB. We can notice how the FD scheme outperforms HD for the majority of values. For instance, the outage probability is very small in HD when $r_{sbs} = 1$ bps/Hz and $r_d < 5$ bps/Hz, but starts increasing when r_d increases since the link TD becomes the worst. For higher values of r_{sbs}, the outage probability even goes to 1 while FD achieves values in the range $10^{-3} - 10^{-1}$. The figure also shows that the optimal FD scheme performs better than the HD case for almost every value of r_d. On the other hand, for fixed configuration, FD approaches the optimal one in only one point. For example, the configuration M = N = 8 is optimal when $r_d = 8$ bps/Hz and $r_{sbs} = 1$ bps/Hz at a path gain of -85 dB. These

results evidence that the FD case with dynamic antenna selection significantly improves the system performance when compared to any fixed case.

Figure 21 shows the worst outage performance achieved when using the un-optimized and dynamic FD schemes. We compared to the simple FD case because according to Figure 20 this one shows better performance than the HD scheme. Then, the bottom surface represents a lower bound for devices working with similar parameters under other transmission schemes. Figure 22 shows a similar approach to the previous but varying the rates at both links for same value of path gain in both cases. Likewise, the dynamic FD proves its supremacy over classical FD.

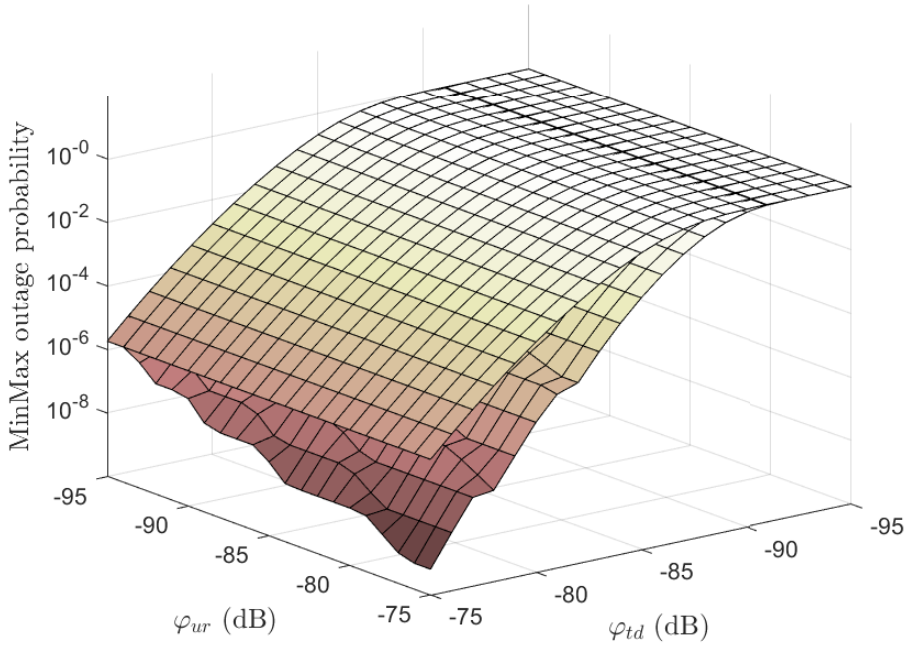

Figure 21. MinMax outage probability in dynamic FD (bottom surface) and FD with fixed number of Tx and Rx antennas (top surface), $r_d = r_{sbs} = 4$ bps/Hz and $Q = 16$.

Figure 23 illustrates the results corresponding to the solution to problem **P2**. Specifically, it shows the minimum number of RF chains required to meet a certain reliability target. By doing this, we guarantee that the performance of the worst link will be always better than the minimum outage requirement. It can be noticed that the outage target is guaranteed with a small number of RF chains even for extreme reliability requirements. From these results, we observe that the rate at the SBS contributes the most to the minimal number of RF chains, thus, larger r_{sbs} requires larger number of RF chains. Meanwhile, as r_d increases, the required number of RF chains increases but slowly. In URC, it is expected that users in the UL have lower rates than in the DL and sacrifice rate towards reliability. Herein, we show that by doing this not only rate and reliability can be guaranteed, but also the number of required resources becomes smaller with respect to needed RF chains.

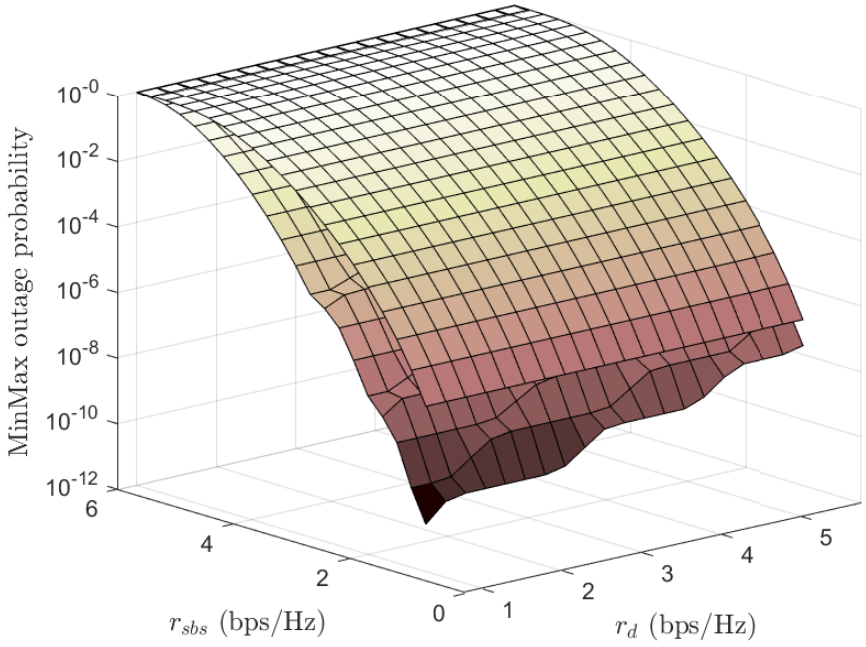

Figure 22. MinMax outage probability in dynamic FD (bottom surface) and FD with fixed number of Tx and Rx antennas (top surface), $\varphi_{\text{td}} = \varphi_{\text{ur}} = -85$ dB and $Q = 16$.

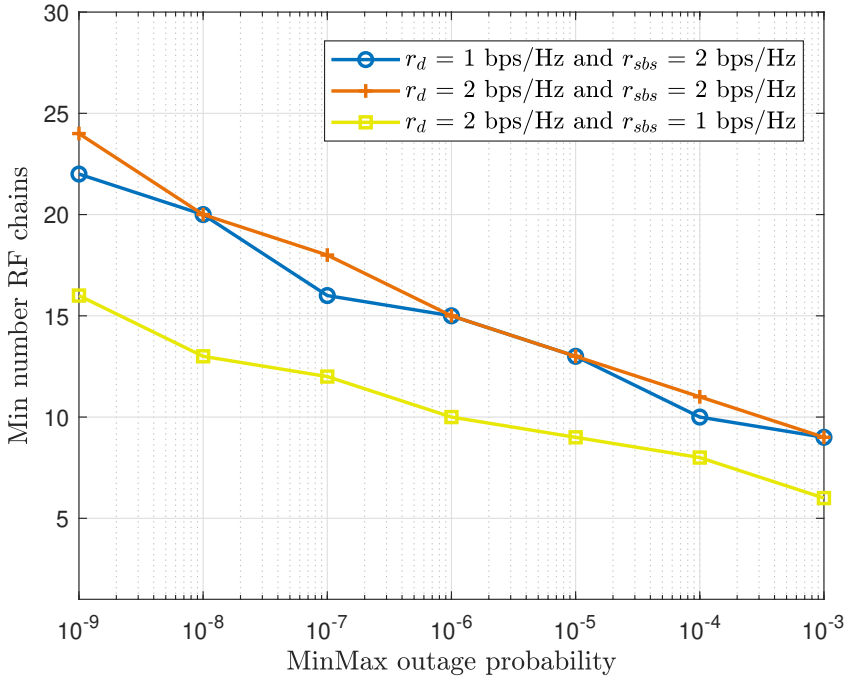

Figure 23. Minimum number of RF chains (Q) required for a given MinMax outage probability target, $\varphi_{\text{ur}} = \varphi_{\text{ud}} = -85$ dB.

5 CONCLUSIONS

This work focused on the use of FD communications, sER and multi-antenna strategies and the benefits of their combined use in terms of reliability. We studied the basic concepts of these technologies that will push forward the implementation of new generations of mobile communications since they bring improvements not only in terms reliability but also spectral and energy efficiencies. We analyzed the advantages of a FD scheme over its HD counterpart and emphasized the use of spatial diversity over frequency and time diversity schemes. Furthermore, we analyzed the performance in terms of fair reliability of a scenario where a SBS serves one UL and one DL device under quasi-static Rayleigh fading. We derived expressions for the outage probability for both channels under HD and FD modes. We also analyzed the difference in the outage probabilities introduced when considering the power consumed by the hardware at the SBS with respect to the ideal case where all the power is considered for transmission. Moreover, we proposed a dynamic FD scheme where the BS adjusts the number of transmit and receive antennas in order to achieve the best performance. We showed that this proposal outperforms simple FD and HD schemes with fixed number of antennas. We also analyzed the impact of the use of sER at the BS side, and proved that the optimal number of transmit and receive antennas that achieves the fairest performance of both DL and UL outages probabilities varies under different network configurations. We also showed how a given target reliability can be imposed to the network by finding a minimum number of RF chains that guarantees an optimum operation in both links under URC constraints. In future works, we could extend this dynamic model to scenarios where the number of UL and DL devices is larger, also by considering larger antenna arrays. We could also include measurements using software defined radios for more practical results.

6 REFERENCES

[1] Mahmood N.H., Böcker S., Munari A., Clazzer F., Moerman I., Mikhaylov K., Lopez O., Park O.S., Mercier E., Bartz H. et al. (2020) White paper on critical and massive machine type communication towards 6G. arXiv preprint arXiv:2004.14146

[2] Li S., Da Xu L. & Zhao S. (2018) 5G Internet of Things: A survey. Journal of Industrial Information Integration 10, pp. 1–9.

[3] Ullah H., Nair N.G., Moore A., Nugent C., Muschamp P. & Cuevas M. (2019) 5G communication: an overview of vehicle-to-everything, drones, and healthcare use-cases. IEEE Access 7, pp. 37251–37268.

[4] Boban M., Kousaridas A., Manolakis K., Eichinger J. & Xu W. (2017) Use cases, requirements, and design considerations for 5G V2X. arXiv preprint arXiv:1712.01754.

[5] Schulz P., Matthe M., Klessig H., Simsek M., Fettweis G., Ansari J., Ashraf S.A., Almeroth B., Voigt J., Riedel I. et al. (2017) Latency critical IoT applications in 5G: Perspective on the design of radio interface and network architecture. IEEE Communications Magazine 55, pp. 70–78.

[6] Liolis K., Geurtz A., Sperber R., Schulz D., Watts S., Poziopoulou G., Evans B., Wang N., Vidal O., Tiomela Jou B. et al. (2019) Use cases and scenarios of 5G integrated satellite-terrestrial networks for enhanced mobile broadband: The SaT5G approach. International Journal of Satellite Communications and Networking 37, pp. 91–112.

[7] Osseiran A., Boccardi F., Braun V., Kusume K., Marsch P., Maternia M., Queseth O., Schellmann M., Schotten H., Taoka H. et al. (2014) Scenarios for 5G mobile and wireless communications: the vision of the METIS project. IEEE communications magazine 52, pp. 26–35.

[8] Popovski P., Nielsen J.J., Stefanovic C., De Carvalho E., Strom E., Trillingsgaard K.F., Bana A.S., Kim D.M., Kotaba R., Park J. et al. (2018) Wireless access for ultra-reliable low-latency communication: Principles and building blocks. IEEE Network 32, pp. 16–23.

[9] Popovski P., Stefanović Č., Nielsen J.J., De Carvalho E., Angjelichinoski M., Trillingsgaard K.F. & Bana A.S. (2019) Wireless access in Ultra-Reliable Low-Latency Communication (URLLC). IEEE Transactions on Communications 67, pp. 5783–5801.

[10] Frotzscher A., Wetzker U., Bauer M., Rentschler M., Beyer M., Elspass S. & Klessig H. (2014) Requirements and current solutions of wireless communication in industrial automation. In: IEEE International Conference on Communications Workshops (ICC), pp. 67–72.

[11] Bennis M., Debbah M. & Poor H.V. (2018) Ultrareliable and low-latency wireless communication: Tail, risk, and scale. Proceedings of the IEEE 106, pp. 1834–1853.

[12] Tabikh W., Yuan-Wu Y. & Slock D. (2017) Beamforming design with combined channel estimate and covariance CSIT via random matrix theory. In: 2017 IEEE International Conference on Communications (ICC), IEEE, pp. 1–5.

[13] Björnson E., Sanguinetti L. & Debbah M. (2016) Massive MIMO with imperfect channel covariance information. In: 50th Asilomar Conference on Signals, Systems and Computers, IEEE, pp. 974–978.

[14] Björnson E., Hammarwall D., Zakhour R., Bengtsson M., Gesbert D. & Ottersten B. (2008) Feedback design in multiuser MIMO systems using quantization splitting and hybrid instantaneous/statistical channel information. In: ICT-MobileSummit Conference, IIMC International Information Management Corporation.

[15] Park J., Samarakoon S., Shiri H., Abdel-Aziz M.K., Nishio T., Elgabli A. & Bennis M. (2020) Extreme URLLC: Vision, challenges, and key enablers. arXiv preprint arXiv:2001.09683.

[16] Nouri P., Alves H., Uusitalo M.A., López O.A. & Latva-aho M. (2020) Machine-type wireless communications enablers for beyond 5G: enabling URLLC via diversity under hard deadlines. Computer Networks , p. 107227.

[17] Zorbas D. & Douligeris C. (2018) Computing optimal drone positions to wirelessly recharge IoT devices. In: IEEE INFOCOM 2018-IEEE Conference on Computer Communications Workshops (INFOCOM WKSHPS), IEEE, pp. 628–633.

[18] Sarker V.K., Queralta J.P., Gia T.N., Tenhunen H. & Westerlund T. (2019) A survey on LoRa for IoT: Integrating edge computing. In: Fourth International Conference on Fog and Mobile Edge Computing (FMEC), IEEE, pp. 295–300.

[19] Popli S., Jha R.K. & Jain S. (2018) A survey on energy efficient narrowband Internet of Things (NBIoT): architecture, application and challenges. IEEE Access 7, pp. 16739–16776.

[20] Ndih E.D.N. & Cherkaoui S. (2016) On enhancing technology coexistence in the IoT era: Zigbee and 802.11 case. IEEE Access 4, pp. 1835–1844.

[21] Buzzi S., Chih-Lin I., Klein T.E., Poor H.V., Yang C. & Zappone A. (2016) A survey of energy-efficient techniques for 5G networks and challenges ahead. IEEE Journal on Selected Areas in Communications 34, pp. 697–709.

[22] Venturino L., Zappone A., Risi C. & Buzzi S. (2014) Energy-efficient scheduling and power allocation in downlink OFDMA networks with base station coordination. IEEE transactions on wireless communications 14, pp. 1–14.

[23] Joung J., Ho C.K., Adachi K. & Sun S. (2014) A survey on power-amplifier-centric techniques for spectrum-and energy-efficient wireless communications. IEEE Communications Surveys & Tutorials 17, pp. 315–333.

[24] Mahmood F., Perrins E. & Liu L. (2015) Modeling and analysis of energy consumption for RF transceivers in wireless cellular systems. In: IEEE Global Communications Conference (GLOBECOM), IEEE, pp. 1–6.

[25] Liu J., Xiong K., Lu Y., Ng D.W.K., Zhong Z. & Han Z. (2020) Energy efficiency in secure IRS-aided SWIPT. IEEE Wireless Communications Letters 9, pp. 1884–1888.

[26] Fang F., Xu Y., Pham Q.V. & Ding Z. (2020) Energy-efficient design of IRS-NOMA networks. IEEE Transactions on Vehicular Technology 69, pp. 14088–14092.

[27] Zhou S., Xu W., Wang K., Di Renzo M. & Alouini M.S. (2020) Spectral and energy efficiency of IRS-assisted MISO communication with hardware impairments. IEEE wireless communications letters 9, pp. 1366–1369.

[28] Nguyen L.D. (2018) Resource allocation for energy efficiency in 5G wireless networks. EAI Endorsed Transactions on Industrial Networks and Intelligent Systems 5.

[29] Li S., Ni Q., Sun Y., Min G. & Al-Rubaye S. (2018) Energy-efficient resource allocation for industrial cyber-physical IoT systems in 5G era. IEEE Transactions on Industrial Informatics 14, pp. 2618–2628.

[30] Munir H., Hassan S.A., Pervaiz H., Ni Q. & Musavian L. (2016) Energy efficient resource allocation in 5G hybrid heterogeneous networks: A game theoretic approach. In: IEEE 84th vehicular technology conference (VTC-Fall), IEEE, pp. 1–5.

[31] Ali S., Ahmad A. & Khan A. (2019) Energy-efficient resource allocation and RRH association in multitier 5G H-CRANs. Transactions on Emerging Telecommunications Technologies 30, p. e3521.

[32] Cetinkaya O., Balsamo D. & Merrett G.V. (2020) Internet of MIMO things: UAV-assisted wireless-powered networks for future smart cities. IEEE Internet of Things Magazine 3, pp. 8–13.

[33] Sodhro A.H., Chen L., Sekhari A., Ouzrout Y. & Wu W. (2018) Energy efficiency comparison between data rate control and transmission power control algorithms for wireless body sensor networks. International Journal of Distributed Sensor Networks 14, p. 1550147717750030.

[34] Wen M., Cheng X. & Yang L. (2014) Optimizing the energy efficiency of OFDM with index modulation. In: IEEE International Conference on Communication Systems, IEEE, pp. 31–35.

[35] Naeem M., Illanko K., Karmokar A., Anpalagan A. & Jaseemuddin M. (2013) Energy-efficient cognitive radio sensor networks: Parametric and convex transformations. Sensors 13, pp. 11032–11050.

[36] Wang S. & Nie J. (2010) Energy efficiency optimization of cooperative communication in wireless sensor networks. EURASIP Journal on Wireless Communications and Networking 2010, pp. 1–8.

[37] Al-Obiedollah H.M., Cumanan K., Thiyagalingam J., Burr A.G., Ding Z. & Dobre O.A. (2019) Energy efficient beamforming design for MISO non-orthogonal multiple access systems. IEEE Transactions on Communications 67, pp. 4117–4131.

[38] Moghadam N.N., Fodor G., Bengtsson M. & Love D.J. (2018) On the energy efficiency of MIMO hybrid beamforming for millimeter-wave systems with nonlinear power amplifiers. IEEE Transactions on Wireless Communications 17, pp. 7208–7221.

[39] Ojo M., Giordano S., Portaluri G., Adami D. & Pagano M. (2017) An energy efficient centralized scheduling scheme in TSCH networks. In: IEEE international conference on communications workshops (ICC workshops), IEEE, pp. 570–575.

[40] Agarwal M.M., Govil M.C., Sinha M. & Gupta S. (2019) Fuzzy based data fusion for energy efficientInternet of Things. International Journal of Grid and High Performance Computing (IJGHPC) 11, pp. 46–58.

[41] Kozłowski A. & Sosnowski J. (2019) Energy efficiency trade-off between duty-cycling and wake-up radio techniques in IoT networks. Wireless Personal Communications 107, pp. 1951–1971.

[42] Dhall R. & Agrawal H. (2018) An improved energy efficient duty cycling algorithm for IoT based precision agriculture. Procedia Computer Science 141, pp. 135–142.

[43] Huang J., Duan Q., Xing C.C. & Wang H. (2017) Topology control for building a large-scale and energy-efficient Internet of Things. IEEE Wireless Communications 24, pp. 67–73.

[44] Trotta A., Di Felice M., Bononi L., Natalizio E., Perilli L., Scarselli E.F., Cinotti T.S. & Canegallo R. (2019) Bee-drones: Energy-efficient data collection on wake-up radio-based wireless sensor networks. In: IEEE INFOCOM IEEE Conference on Computer Communications Workshops (INFOCOM WKSHPS), IEEE, pp. 547–553.

[45] Gupta S.K., Kuila P. & Jana P.K. (2016) Energy efficient multipath routing for wireless sensor networks: A genetic algorithm approach. In: International conference on advances in computing, communications and informatics (ICACCI), IEEE, pp. 1735–1740.

[46] Wang L., Yang Y. & Zhao W. (2012) Network coding-based multipath routing for energy efficiency in wireless sensor networks. EURASIP Journal on Wireless Communications and Networking 2012, pp. 1–15.

[47] Lin Y., Zhang R., Yang L. & Hanzo L. (2018) Secure user-centric clustering for energy efficient ultra-dense networks: Design and optimization. IEEE Journal on Selected Areas in Communications 36, pp. 1609–1621.

[48] Park S., Lee W. & Cho D.h. (2012) Fair clustering for energy efficiency in a cooperative wireless sensor network. In: IEEE 75th Vehicular Technology Conference (VTC Spring), IEEE, pp. 1–5.

[49] Mafuta A.D., Walingo T. & Ngatched T.M. (2017) Energy efficient coverage extension relay node placement in LTE-A networks. IEEE Communications Letters 21, pp. 1617–1620.

[50] Xiang L., Luo J. & Vasilakos A. (2011) Compressed data aggregation for energy efficient wireless sensor networks. In: 8th annual IEEE communications society conference on sensor, mesh and ad-hoc communications and networks, IEEE, pp. 46–54.

[51] Jiang D., Xu Z., Li W. & Chen Z. (2015) Network coding-based energy-efficient multicast routing algorithm for multi-hop wireless networks. Journal of Systems and Software 104, pp. 152–165.

[52] Vu T.T., Ngo D.T., Dao M.N., Durrani S., Nguyen D.H. & Middleton R.H. (2018) Energy efficiency maximization for downlink cloud radio access networks with data sharing and data compression. IEEE Transactions on Wireless Communications 17, pp. 4955–4970.

[53] Kishore R.A. & Priya S. (2018) A review on low-grade thermal energy harvesting: materials, methods and devices. Materials 11, p. 1433.

[54] Hamlehdar M., Kasaeian A. & Safaei M.R. (2019) Energy harvesting from fluid flow using piezoelectrics: A critical review. Renewable Energy 143, pp. 1826–1838.

[55] Zeadally S., Shaikh F.K., Talpur A. & Sheng Q.Z. (2020) Design architectures for energy harvesting in the Internet of Things. Renewable and Sustainable Energy Reviews 128, p. 109901.

[56] Bi S., Ho C.K. & Zhang R. (2015) Wireless powered communication: Opportunities and challenges. IEEE Communications Magazine 53, pp. 117–125.

[57] Lu X., Wang P., Niyato D., Kim D.I. & Han Z. (2015) Wireless charging technologies: Fundamentals, standards, and network applications. IEEE Communications Surveys & Tutorials 18, pp. 1413–1452.

[58] Li X., Tsui C.Y. & Ki W.H. (2015) A 13.56 MHz wireless power transfer system with reconfigurable resonant regulating rectifier and wireless power control for implantable medical devices. IEEE Journal of Solid-State Circuits 50, pp. 978–989.

[59] Dana R., Sardhara P., Sanghani A. & Mehta P. (2020) A detailed survey of rectenna for energy harvesting: Over a wide range of frequency. In: Optical and Wireless Technologies, Springer, pp. 43–55.

[60] Ma G., Xu J., Zeng Y. & Moghadam M.R.V. (2019) A generic receiver architecture for MIMO wireless power transfer with nonlinear energy harvesting. IEEE Signal Processing Letters 26, pp. 312–316.

[61] Sabharwal A., Schniter P., Guo D., Bliss D.W., Rangarajan S. & Wichman R. (2014) In-band full-duplex wireless: Challenges and opportunities. IEEE Journal on selected areas in communications 32, pp. 1637–1652.

[62] Duarte M., Dick C. & Sabharwal A. (2012) Experiment-driven characterization of full-duplex wireless systems. IEEE Transactions on Wireless Communications 11, pp. 4296–4307.

[63] Choi J.I., Hong S., Jain M., Katti S., Levis P. & Mehlman J. (2012) Beyond full-duplex wireless. In: Conference Record of the Forty Sixth Asilomar Conference on Signals, Systems and Computers (ASILOMAR), IEEE, pp. 40–44.

[64] Bharadia D., McMilin E. & Katti S. (2013) Full duplex radios. In: Proceedings of the ACM SIGCOMM conference on SIGCOMM, pp. 375–386.

[65] Alves H., Souza R.D. & Pellenz M.E. (2015) Brief survey on full-duplex relaying and its applications on 5G. In: IEEE 20th International Workshop on Computer Aided Modelling and Design of Communication Links and Networks (CAMAD), IEEE, pp. 17–21.

[66] Zhang Z., Long K., Vasilakos A.V. & Hanzo L. (2016) Full-duplex wireless communications: Challenges, solutions, and future research directions. Proceedings of the IEEE 104, pp. 1369–1409.

[67] Nwankwo C.D., Zhang L., Quddus A., Imran M.A. & Tafazolli R. (2017) A survey of self-interference management techniques for single frequency full duplex systems. IEEE Access 6, pp. 30242–30268.

[68] Zhou J., Chuang T.H., Dinc T. & Krishnaswamy H. (2015) Integrated wideband self-interference cancellation in the RF domain for FDD and full-duplex wireless. IEEE Journal of Solid-State Circuits 50, pp. 3015–3031.

[69] Askar R., Kaiser T., Schubert B., Haustein T. & Keusgen W. (2014) Active self-interference cancellation mechanism for full-duplex wireless transceivers. In: 2014 9th International Conference on Cognitive Radio Oriented Wireless Networks and Communications (CROWNCOM), IEEE, pp. 539–544.

[70] Ahmed E., Eltawil A.M. & Sabharwal A. (2013) Self-interference cancellation with nonlinear distortion suppression for full-duplex systems. In: 2013 Asilomar Conference on Signals, Systems and Computers, IEEE, pp. 1199–1203.

[71] Korpi D., Anttila L., Syrjälä V. & Valkama M. (2014) Widely linear digital self-interference cancellation in direct-conversion full-duplex transceiver. IEEE Journal on Selected Areas in Communications 32, pp. 1674–1687.

[72] Riihonen T. & Wichman R. (2012) Analog and digital self-interference cancellation in full-duplex MIMO-OFDM transceivers with limited resolution in A/D conversion. In: Conference record of the forty sixth asilomar conference on signals, systems and computers (ASILOMAR), IEEE, pp. 45–49.

[73] Sim M.S., Chung M., Kim D., Chung J., Kim D.K. & Chae C.B. (2017) Nonlinear self-interference cancellation for full-duplex radios: From link-level and system-level performance perspectives. IEEE Communications Magazine 55, pp. 158–167.

[74] Balatsoukas-Stimming A. (2018) Non-linear digital self-interference cancellation for in-band full-duplex radios using neural networks. In: IEEE 19th International Workshop on Signal Processing Advances in Wireless Communications (SPAWC), IEEE, pp. 1–5.

[75] Khaledian S., Farzami F., Smida B. & Erricolo D. (2018) Inherent self-interference cancellation for in-band full-duplex single-antenna systems. IEEE Transactions on Microwave Theory and Techniques 66, pp. 2842–2850.

[76] Dastjerdi M.B., Reiskarimian N., Chen T., Zussman G. & Krishnaswamy H. (2018) Full duplex circulator-receiver phased array employing self-interference cancellation via beamforming. In: IEEE Radio Frequency Integrated Circuits Symposium (RFIC), IEEE, pp. 108–111.

[77] Korpi D., Heino M., Icheln C., Haneda K. & Valkama M. (2016) Compact inband full-duplex relays with beyond 100 dB self-interference suppression: Enabling techniques and field measurements. IEEE Transactions on Antennas and Propagation 65, pp. 960–965.

[78] Shojaeifard A., Wong K.K., Di Renzo M., Zheng G., Hamdi K.A. & Tang J. (2017) Self-interference in full-duplex multi-user MIMO channels. IEEE Communications Letters 21, pp. 841–844.

[79] Duarte M. (2012) Full-duplex wireless: Design, implementation and characterization. Ph.D. thesis.

[80] Alves H., da Costa D.B., Souza R.D. & Latva-aho M. (2013) Performance of block-markov full-duplex relaying with self interference in Nakagami-m fading. IEEE Wireless Communications Letters 2, pp. 311–314.

[81] Irio L. & Oliveira R. (2019) Distribution of the residual self-interference power in in-band full-duplex wireless systems. IEEE Access 7, pp. 57516–57526.

[82] Zheng G., Krikidis I., Li J., Petropulu A.P. & Ottersten B. (2013) Improving physical layer secrecy using full-duplex jamming receivers. IEEE Transactions on Signal Processing 61, pp. 4962–4974.

[83] Sahai A., Patel G., Dick C. & Sabharwal A. (2013) On the impact of phase noise on active cancelation in wireless full-duplex. IEEE transactions on Vehicular Technology 62, pp. 4494–4510.

[84] Aryafar E., Khojastepour M.A., Sundaresan K., Rangarajan S. & Chiang M. (2012) MIDU: Enabling MIMO full-duplex. In: Proceedings of the 18th annual international conference on mobile computing and networking, pp. 257–268.

[85] Haneda K., Kahra E., Wyne S., Icheln C. & Vainikainen P. (2010) Measurement of loop-back interference channels for outdoor-to-indoor full-duplex radio relays. In: Proceedings of the Fourth European Conference on Antennas and Propagation, IEEE, pp. 1–5.

[86] Khojastepour M.A., Sundaresan K., Rangarajan S., Zhang X. & Barghi S. (2011) The case for antenna cancellation for scalable full-duplex wireless communications. In: Proceedings of the 10th ACM Workshop on Hot Topics in Networks, pp. 1–6.

[87] Dinc T. & Krishnaswamy H. (2015) AT/R antenna pair with polarization-based reconfigurable wideband self-interference cancellation for simultaneous transmit and receive. In: IEEE MTT-S International Microwave Symposium, IEEE, pp. 1–4.

[88] Askar R., Sarmadi M.M., Undi F., Peter M., Keusgen W. & Haustein T. (2019) Time dispersion characteristics of cross-polarized 2x2 MIMO self-interference indoor radio channels. In: IEEE 90th Vehicular Technology Conference (VTC2019-Fall), IEEE, pp. 1–6.

[89] Zeng Y. & Zhang R. (2014) Optimized training design for wireless energy transfer. IEEE Transactions on Communications 63, pp. 536–550.

[90] López O.L.A., Alves H., Souza R.D., Montejo-Sánchez S., Fernández E.M.G. & Latva-aho M. (2019) Massive wireless energy transfer: Enabling sustainable IoT towards 6G era. arXiv preprint arXiv:1912.05322.

[91] Kostoff R.N., Heroux P., Aschner M. & Tsatsakis A. (2020) Adverse health effects of 5G mobile networking technology under real-life conditions. Toxicology Letters 323, pp. 35–40.

[92] He W., Xu B., Gustafsson M., Ying Z. & He S. (2017) RF compliance study of temperature elevation in human head model around 28 GHz for 5G user equipment application: Simulation analysis. IEEE Access 6, pp. 830–838.

[93] Rosabal O.M., López O.L.A., Alves H., Montejo-Sánchez S. & Latva-aho M. (2020) On the optimal deployment of power beacons for massive wireless energy transfer. IEEE Internet of Things Journal.

[94] Zeng Y., Clerckx B. & Zhang R. (2017) Communications and signals design for wireless power transmission. IEEE Transactions on Communications 65, pp. 2264–2290.

[95] Clerckx B., Huang K., Varshney L.R., Ulukus S. & Alouini M.S. (2021) Wireless Power Transfer for Future Networks: Signal Processing, Machine Learning, Computing, and Sensing. arXiv preprint arXiv:2101.04810.

[96] Chen X., Yuen C. & Zhang Z. (2013) Wireless energy and information transfer tradeoff for limited-feedback multiantenna systems with energy beamforming. IEEE Transactions on Vehicular Technology 63, pp. 407–412.

[97] Yang G., Ho C.K. & Guan Y.L. (2014) Dynamic resource allocation for multiple-antenna wireless power transfer. IEEE Transactions on Signal Processing 62, pp. 3565–3577.

[98] Son H. & Clerckx B. (2014) Joint beamforming design for multi-user wireless information and power transfer. IEEE Transactions on Wireless Communications 13, pp. 6397–6409.

[99] Park J. & Clerckx B. (2015) Joint wireless information and energy transfer with reduced feedback in MIMO interference channels. IEEE Journal on Selected Areas in Communications 33, pp. 1563–1577.

[100] Xu J. & Zhang R. (2014) Energy beamforming with one-bit feedback. IEEE Transactions on Signal Processing 62, pp. 5370–5381.

[101] Abeywickrama S., Samarasinghe T., Ho C.K. & Yuen C. (2017) Wireless energy beamforming using received signal strength indicator feedback. IEEE Transactions on Signal Processing 66, pp. 224–235.

[102] Lee S., Zeng Y. & Zhang R. (2017) Retrodirective multi-user wireless power transfer with massive MIMO. IEEE Wireless Communications Letters 7, pp. 54–57.

[103] Ju H. & Zhang R. (2013) Throughput maximization in wireless powered communication networks. IEEE Transactions on Wireless Communications 13, pp. 418–428.

[104] Wu Q., Chen W., Ng D.W.K. & Schober R. (2018) Spectral and energy-efficient wireless powered IoT networks: NOMA or TDMA? IEEE Transactions on Vehicular Technology 67, pp. 6663–6667.

[105] Chi K., Chen Z., Zheng K., Zhu Y.h. & Liu J. (2019) Energy provision minimization in wireless powered communication networks with network throughput demand: TDMA or NOMA? IEEE Transactions on Communications 67, pp. 6401–6414.

[106] Liu L., Zhang R. & Chua K.C. (2014) Multi-antenna wireless powered communication with energy beamforming. IEEE Transactions on Communications 62, pp. 4349–4361.

[107] Lim H. & Hwang T. (2018) User-centric energy efficiency optimization for MISO wireless powered communications. IEEE Transactions on Wireless Communications 18, pp. 864–878.

[108] Ju H. & Zhang R. (2014) Optimal resource allocation in full-duplex wireless-powered communication network. IEEE Transactions on Communications 62, pp. 3528–3540.

[109] Zhou X., Zhang R. & Ho C.K. (2013) Wireless information and power transfer: Architecture design and rate-energy tradeoff. IEEE Transactions on communications 61, pp. 4754–4767.

[110] Liu T., Wang X. & Zheng L. (2017) A cooperative SWIPT scheme for wirelessly powered sensor networks. IEEE Transactions on Communications 65, pp. 2740–2752.

[111] Xu D. & Li Q. (2019) Resource allocation in OFDM-based wireless powered communication networks with SWIPT. AEU-International Journal of Electronics and Communications 101, pp. 69–75.

[112] Tang J., Luo J., Liu M., So D.K., Alsusa E., Chen G., Wong K.K. & Chambers J.A. (2019) Energy efficiency optimization for NOMA with SWIPT. IEEE Journal of Selected Topics in Signal Processing 13, pp. 452–466.

[113] Zeng Y. & Zhang R. (2015) Full-duplex wireless-powered relay with self-energy recycling. IEEE Wireless Communications Letters 4, pp. 201–204.

[114] Hu S., Ding Z. & Ni Q. (2016) Beamforming optimisation in energy harvesting cooperative full-duplex networks with self-energy recycling protocol. IET Communications 10, pp. 848–853.

[115] Wu W., Wang B., Deng Z. & Zhang H. (2016) Secure beamforming for full-duplex wireless powered communication systems with self-energy recycling. IEEE Wireless Communications Letters 6, pp. 146–149.

[116] Hwang D., Hwang K.C., Kim D.I. & Lee T.J. (2016) Self-energy recycling for RF powered multi-antenna relay channels. IEEE Transactions on Wireless Communications 16, pp. 812–824.

[117] Hu Z., Yuan C., Zhu F. & Gao F. (2016) Weighted sum transmit power minimization for full-duplex system with SWIPT and self-energy recycling. IEEE Access 4, pp. 4874–4881.

[118] López O.L.A. & Alves H. (2020) Full duplex and wireless-powered communications. In: Full-Duplex Communications for Future Wireless Networks, Springer, pp. 219–248.

[119] Nethi S., Jäntti R. & Nässi V. (2009) Time and antenna diversity in wireless sensor and actuator networks. In: IEEE 9th Malaysia International Conference on Communications (MICC), IEEE, pp. 932–937.

[120] Tse D. & Viswanath P. (2005) Fundamentals of wireless communication. Cambridge university press.

[121] Goldsmith A. (2005) Wireless communications. Cambridge university press.

[122] Zand P., Chatterjea S., Das K. & Havinga P. (2012) Wireless industrial monitoring and control networks: The journey so far and the road ahead. Journal of sensor and actuator networks 1, pp. 123–152.

[123] Watteyne T., Lanzisera S., Mehta A. & Pister K.S. (2010) Mitigating multipath fading through channel hopping in wireless sensor networks. In: IEEE International Conference on Communications, IEEE, pp. 1–5.

[124] Ortiz J. & Culler D. (2010) Multichannel reliability assessment in real world WSNs. In: Proceedings of the 9th ACM/IEEE International Conference on Information Processing in Sensor Networks, pp. 162–173.

[125] Gonga A., Landsiedel O., Soldati P. & Johansson M. (2012) Multi-channel communication vs. adaptive routing for reliable communication in WSNs. In: ACM/IEEE 11th International Conference on Information Processing in Sensor Networks (IPSN), IEEE, pp. 125–126.

[126] Yang H.C., Choi S. & Alouini M.S. (2019) Ultra-reliable low-latency transmission of small data over fading channels: A data-oriented analysis. IEEE Communications Letters 24, pp. 515–519.

[127] Öhmann D. & Fettweis G.P. (2015) Minimum duration outage of wireless Rayleigh-fading links using selection combining. In: IEEE Wireless Communications and Networking Conference (WCNC), IEEE, pp. 681–686.

[128] Lai X., Fan L., Lei X., Li J., Yang N. & Karagiannidis G.K. (2019) Distributed secure switch-and-stay combining over correlated fading channels. IEEE Transactions on Information Forensics and Security 14, pp. 2088–2101.

[129] López O.L.A., Mahmood N.H. & Alves H. (2020) Enabling URLLC for low-cost IoT devices via diversity combining schemes. In: IEEE International Conference on Communications Workshops (ICC Workshops), IEEE, pp. 1–6.

[130] Berardinelli G., Mahmood N.H., Abreu R., Jacobsen T., Pedersen K., Kovács I.Z. & Mogensen P. (2018) Reliability analysis of uplink grant-free transmission over shared resources. IEEE Access 6, pp. 23602–23611.

[131] Anwar W., Kulkarni K., Franchi N. & Fettweis G. (2018) Physical layer abstraction for ultra-reliable communications in 5G multi-connectivity networks. In: IEEE 29th Annual International Symposium on Personal, Indoor and Mobile Radio Communications (PIMRC), IEEE, pp. 1–6.

[132] López O.L.A., Alves H. & Latva-aho M. (2019) Joint power control and rate allocation enabling ultra-reliability and energy efficiency in SIMO wireless networks. IEEE Transactions on Communications 67, pp. 5768–5782.

[133] López O.L., Mahmood N.H., Alves H., Lima C.M. & Latva-aho M. (2020) Ultra-low latency, low energy, and massiveness in the 6G Era via Efficient CSIT-Limited Scheme. IEEE Communications Magazine 58, pp. 56–61.

[134] Feng C. & Jing Y. (2016) Modified MRT and outage probability analysis for massive MIMO downlink under per-antenna power constraint. In: IEEE 17th International Workshop on Signal Processing Advances in Wireless Communications (SPAWC), IEEE, pp. 1–6.

[135] Ghanem W.R., Jamali V., Sun Y. & Schober R. (2020) Resource allocation for multi-user downlink MISO OFDMA-URLLC systems. IEEE Transactions on Communications 68, pp. 7184–7200.

[136] Lu L., Li G.Y., Swindlehurst A.L., Ashikhmin A. & Zhang R. (2014) An overview of massive MIMO: Benefits and challenges. IEEE journal of selected topics in signal processing 8, pp. 742–758.

[137] Chen H., Dong Z., Zhang J.K. & Vucetic B. (2020) Design of non-orthogonal and noncoherent massive MIMO for scalable URLLC beyond 5G. arXiv preprint arXiv:2001.10728.

[138] Östman J., Lancho A., Durisi G. & Sanguinetti L. (2020) URLLC with Massive MIMO: Analysis and Design at Finite Blocklength. arXiv preprint arXiv:2009.10550.

[139] Zeng J., Lv T., Liu R.P., Su X., Guo Y.J. & Beaulieu N.C. (2019) Enabling ultrareliable and low-latency communications under shadow fading by massive MU-MIMO. IEEE Internet of Things Journal 7, pp. 234–246.

[140] Vu T.K., Liu C.F., Bennis M., Debbah M., Latva-Aho M. & Hong C.S. (2017) Ultra-reliable and low latency communication in mmWave-enabled massive MIMO networks. IEEE Communications Letters 21, pp. 2041–2044.

[141] Yadav A., Dobre O.A. & Poor H.V. (2018) Is self-interference in full-duplex communications a foe or a friend? IEEE Signal Processing Letters 25, pp. 951–955.

[142] Agrawal K., Flanagan M.F. & Prakriya S. (2020) NOMA with battery-assisted energy harvesting full-duplex relay. IEEE Transactions on Vehicular Technology 69, pp. 13952–13957.

[143] Nasir A.A., Tuan H.D., Duong T.Q. & Poor H.V. (2019) Full-duplex MIMO-OFDM communication with self-energy recycling. arXiv preprint arXiv:1903.09931.

[144] Zhai D., Chen H., Lin Z., Li Y. & Vucetic B. (2018) Accumulate then transmit: Multiuser scheduling in full-duplex wireless-powered IoT systems. IEEE Internet of Things Journal 5, pp. 2753–2767.

[145] Zhao X., Zhang Y., Geng S., Du F., Zhou Z. & Yang L. (2019) Hybrid precoding for an adaptive interference decoding SWIPT system with full-duplex IoT devices. IEEE Internet of Things Journal 7, pp. 1164–1177.

[146] Guo J., Zhang S., Zhao N. & Wang X. (2019) Performance of SWIPT for full-duplex relay system with co-channel interference. IEEE Transactions on Vehicular Technology 69, pp. 2311–2315.

[147] López O.L.A., Alves H., Souza R.D. & Fernández E.M.G. (2017) Ultrareliable short-packet communications with wireless energy transfer. IEEE Signal Processing Letters 24, pp. 387–391.

[148] Olver F.W., Lozier D.W., Boisvert R.F. & Clark C.W. (2010) NIST handbook of mathematical functions hardback and CD-ROM. Cambridge university press.

[149] Mickle M.H., Mi M. & Mats L. (2009), Multiple antenna energy harvesting. US Patent 7,528,698.

[150] Jeffrey A. & Zwillinger D. (2007) Table of integrals, series, and products. Elsevier.

[151] Nadarajah S. (2008) On the product of generalized Pareto random variables. Applied Economics Letters 15, pp. 253–259.

[152] Abramowitz M. & Stegun I.A. (1948) Handbook of mathematical functions with formulas, graphs, and mathematical tables, vol. 55. US Government printing office.

[153] Culbertson D.L. & Travelyn R.F. (2003), Full duplex transceiver. US Patent 6,665,276.

[154] Cui S., Goldsmith A.J. & Bahai A. (2004) Energy-efficiency of MIMO and cooperative MIMO techniques in sensor networks. IEEE Journal on Selected Areas in Communications 22, pp. 1089–1098.

[155] Heino M., Korpi D., Huusari T., Antonio-Rodriguez E., Venkatasubramanian S., Riihonen T., Anttila L., Icheln C., Haneda K., Wichman R. et al. (2015) Recent advances in antenna design and interference cancellation algorithms for in-band full duplex relays. IEEE Communications Magazine 53, pp. 91–101.